

CFD SIMULATION OF LIQUID ROCKET ENGINE INJECTORS

Richard Farmer & Gary Cheng
SECA, Inc.

Yen-Sen Chen
ESI, Inc.

INTRODUCTION

Detailed design issues associated with liquid rocket engine injectors and combustion chamber operation require CFD methodology which simulates highly three-dimensional, turbulent, vaporizing, and combusting flows. The primary utility of such simulations involves predicting multi-dimensional effects caused by specific injector configurations. SECA, Inc. and Engineering Sciences, Inc. have been developing appropriate computational methodology for NASA/MSFC for the past decade. CFD tools and computers have improved dramatically during this time period; however, the physical submodels used in these analyses must still remain relatively simple in order to produce useful results. Simulations of clustered coaxial and impinger injector elements for hydrogen and hydrocarbon fuels, which account for real fluid properties, is the immediate goal of this research. The spray combustion codes are based on the FDNS CFD code¹ and are structured to represent homogeneous and heterogeneous spray combustion. The homogeneous spray model treats the flow as a continuum of multi-phase, multicomponent fluids which move without thermal or velocity lags between the phases. Two heterogeneous models were developed: (1) a volume-of-fluid (VOF) model which represents the liquid core of coaxial or impinger jets and their atomization and vaporization, and (2) a Blob model which represents the injected streams as a cloud of droplets the size of the injector orifice which subsequently exhibit particle interaction, vaporization, and combustion. All of these spray models are computationally intensive, but this is unavoidable to accurately account for the complex physics and combustion which is to be predicted. Work is currently in progress to parallelize these codes to improve their computational efficiency.

These spray combustion codes were used to simulate the three test cases which are the subject of the 2nd International Workshop on Rocket Combustion Modeling. Such test cases are considered by these investigators to be very valuable for code validation because combustion kinetics, turbulence models and atomization models based on low pressure experiments of hydrogen air combustion do not adequately verify analytical or CFD submodels which are necessary to simulate rocket engine combustion.

We wish to emphasize that the simulations which we prepared for this meeting are meant to test the accuracy of the approximations used in our general purpose spray combustion models, rather than represent a definitive analysis of each of the experiments which were conducted. Our goal is to accurately predict local temperatures and mixture ratios in rocket engines; hence predicting individual experiments is used only for code validation. To replace the conventional JANNAF standard axisymmetric finite-rate (TDK) computer code² for performance prediction with CFD cases, such codes must possess two features. Firstly, they must be as easy to use and of comparable run times for conventional performance predictions. Secondly, they must provide more detailed predictions of the

flowfields near the injector face. Specifically, they must accurately predict the convective mixing of injected liquid propellants in terms of the injector element configurations.

METHODOLOGY

Homogeneous Spray Combustion Model

The homogeneous spray combustion CFD codes utilize very general thermodynamics in a conventional CFD code. The heterogeneous codes use tabulated properties for the liquid phase and ideal gas properties for the vapor phase. Thermal and caloric equations of state, vapor pressure, heat of vaporization, surface tension, and transport properties are modeled with the equations of state proposed by Hirshfelder, et al^{3,4} (we term these the HBMS equations of state) and with conventional correlations,⁵ for the other properties. The property correlations used were not chosen for their absolute accuracy, but for their validity over a wide range of temperatures and pressures and for requiring a minimum of data to describe a particular species. These correlations are explicit in density and temperature.

HBMS thermal equation of state:

$$\frac{P}{P_c} = \sum_{j=1}^4 T_r^{j-2} \sum_{i=1}^6 B_{ij} \rho_r^{i-2} ; T_r = \frac{T}{T_c} ; \rho_r = \frac{\rho}{\rho_c}$$

HBMS caloric equation of state:

$$\frac{H - H_0}{RT} = Z_c \int_0^{\rho_r} \left[\frac{P}{T_r} - \left(\frac{\partial P}{\partial T_r} \right)_{\rho_r} \right] \rho_r^{-2} d\rho_r + Z_c \frac{P}{\rho_r T_r} - 1$$

These equations are based on the "theorem of corresponding states" for real fluids, which essentially means that the p-v-T relations for all species are similar if these variables are normalized with their values at the critical point, i.e. if reduced values are used. The reduced values in these equations are indicated with a subscript r. H_0 is the ideal gas species enthalpy. Z_c is the compressibility for a given species at the critical point. The HBMS equations are attractive to use because arbitrary correlations for vapor pressure, heat of vaporization, and liquid densities can be used. Since multi-component fluid/vapor mixtures may be present in the flowfield, the mixture properties are calculated by the additive volume method. This means that multiphase mixtures are treated as ideal solutions. For H_2/O_2 propellants under conditions where the species become ideal gases, the thermodynamic data from the CEC code⁶ were used.

The combustion reactions used in the simulations reported herein are shown in Table 1. Not all of the reactions were used in all of the combustion simulations. Elementary rate data for these reactions are reported by Gardner, et al^{7,8}. Such data are empirical and were obtained for hydrogen/air combustion, under conditions far different from those encountered in rocket engines.

Table 1. Combustion Model for H₂/O₂ Reaction

<p>Chain initiation: $H_2 + O_2 = 2OH$ $1.86 H_2 + O_2 = 1.645 H_2O + 0.067 O + 0.142 H + 0.288 OH$</p>
<p>Chain Branching: $H_2 + OH = H_2O + H$ $2 OH = H_2O + O$ $H_2 + O = H + OH$ $O_2 + H = O + OH$</p>
<p>Chain termination: $O + H + M = OH + M$ $2 O + M = O_2 + M$ $2 H + M = H_2 + M$ $OH + H + M = H_2O + M$</p>

The CFD solver used was the Finite-Difference Navier-Stokes code with provision for using real fluid properties, the FDNS-RFV code. This code is pressure based; it differs from an ideal gas code in the methodology used to relate the pressure correction to the continuity equation and of course in the properties subroutines used. The pressure correction (p') equation used in the FDNS-RFV code is:

$$\frac{\beta_p p'}{\Delta T} \Delta \cdot (u_i \beta_p p') - \Delta \cdot (\rho^* D_p \Delta p') = -\Delta \cdot (\rho^* u_i) - \frac{\rho^* - \rho^n}{\Delta t}$$

$$p^{n+1} = p^n + p'; \quad \beta_p = \gamma/a^2; \quad u_i \approx -D_p \Delta p'$$

where the superscripts * and n denote the value at the intermediate and previous time steps, respectively. D_p is the inverse of the matrix of the coefficients of the convective terms in the finite-difference form of the inviscid equations of motion. This is not an obvious definition, but is one which has made the FDNS-RFV code a useful solver. The sound speed used in the pressure correction equation is that calculated for the real fluid multi-component mixture.

In all cases simulated, a k- ϵ turbulence model was used to close the mass averaged transport equations solved by the code. Our experience is that this incompressible turbulence model overestimates the mixing in a combusting flowfield. However, since the liquid propellants are also mixed by this model, we concluded that there are currently insufficient data to better tune the turbulence model. The homogeneous spray model has been used to simulate: (1) a single element like-on-like (LOL) impinger injector element and a single element unlike impinger element for the configuration and flow conditions used in the cold-flow experiments; (2) an ensemble of injector elements in the Fastrac engine; and (3) several configurations of the vortex engine currently being developed.⁹

Heterogeneous Spray Combustion Model

Simulations of shear coaxial injector combustion may include models that characterize the breakup or atomization of the round liquid jet, subsequent droplet secondary breakup, turbulence dispersion, droplet evaporation and gas-phase mixing and combustion. The primary atomization rate of the liquid jet is modeled following the work of Reitz and Diwakar¹⁰. Applications of this model to shear coaxial injector test cases, with a volume-of-fluid equation to model the liquid fuel/oxidizer jets, were presented by Chen, et al.¹¹. For the present application, since the liquid core length and the initial droplet size are specified, the primary atomization model is therefore ignored.

Particulate Two-Phase Flow Model

The two-phase interactions are important throughout the life history of the droplets. In the initial phase of injection, momentum and energy exchanges through the drag forces and heat transfer are dominating. These inter-phase transfer terms appear in the Navier-Stokes equations that are solved using the present CFD flow solver. Mass transfer occurs as the particles are heated through the surrounding hot gas. Mean gas-phase properties and turbulence eddy properties are used for the statistical droplet tracking calculations.

Droplet Secondary Breakup Model

The TAB (Taylor Analogy Breakup) model of O'Rourke and Amsden¹² is based on an analogy between an oscillating and distorting droplet and a spring-mass system. The restoring force of the spring is analogous to the surface tension forces on the droplet surface. The external force on the mass is analogous to the gas aerodynamic force. The damping forces due to liquid viscosity are introduced also based on this model.

Droplet-Turbulence Interaction

A two-equation turbulence model is used to characterize the flowfield turbulence quantities, such as turbulence fluctuations, eddy life time and length scale. Turbulent effects on particles are modeled by assuming the influence of velocity fluctuations on the particles creates statistical dispersion of the particles. The velocity fluctuations, which are calculated from the solutions of the turbulence kinetic energy, are assumed to follow a Gaussian distribution with standard deviation proportional to the square root of turbulence kinetic energy. This magnitude of this statistical particle dispersion is then transported following the trajectory of the particles with their radii of influence within which coupling effects (also follow the Gaussian distribution) between two phases occur. This method is classified as the parcel PDF (cloud) model, by Shang¹³, for turbulent particle dispersion. As oppose to the stochastic separated flow (SSF) model, the number of computational particles required is drastically reduced for the same statistical representation of the spray. This provides great savings in computational effort in performing the spray combustion computations.

Droplet Evaporation Model

The droplet evaporation rates and the droplet heat-up rates are determined using the general evaporation model of Schuman¹⁴, which is continuously valid from subcritical to supercritical conditions. This vaporization model was extended from the classical approach¹⁵, by neglecting the effects of solubility of the surrounding gas into the droplet. However, this approach satisfies the global transient film continuity equation for the drop vapor and the ambient gas to obtain the expressions consistent for the molar flow rates.

Chemical Reaction Model

A finite-rate chemistry model with point-implicit integration method is employed in the present study. A 9-reaction kinetics model of Anon¹⁶ is used for modeling the H₂-O₂ combustion. The initiation reaction used produced OH. This chemistry model is listed in Table 1.

SIMULATIONS OF THE RCM-1 EXPERIMENTS

The LN2 cases, RCM-1-A and -B, were simulated with the homogeneous spray model. The flow predicted resembles a dense fluid jet with strong density gradients in the shear layer. Such a flow has been observed in a similar super-critical nitrogen jet experiment reported by Chehroudi, et al¹⁷. These predictions should compare well to the DLR experimental data. If the comparisons are not good, adjustment of the parameters in the two-equation $k-\epsilon$ or the initial turbulence level parameters could be made for a better fit of the data. Such tuning has not previously been made since appropriate test data were not available. For a definitive analysis of the experiments, conjugate heat transfer to the injector hardware and consideration of the duration of the experiment should be made. The jet is discharging into a gaseous nitrogen environment, the recirculated gas should become slowly cooled until a steady state is reached. Since the temporal variation of the recirculating gas temperature was not reported, the time that the CFD simulation should be terminated can not be determined. Since the measurements were made very close to the injector exit, good simulation of the gas temperature might not be crucially important.

The injector configuration and flow conditions for the cryogenic nitrogen jet of the RCM-1 test cases are illustrated in Fig. 1. It can be seen that the chamber pressure for both cases is above the critical pressure of nitrogen. A 101x11-mesh system was used to discretize the injector section, while the chamber section was modeled by a 301x101-mesh system for Case RCM-1-A. The same grid system was used to simulate both RCM-1-A and RCM-1-B test cases. The numerical result of RCM-1-A test case at the locations specified by IWRCM was plotted as shown in Figures 2-6. Notice the temperature profiles in Figure 4. These two cold flow cases are not steady-state, although the simulations assumed this to be the situation. The simulations presented represent a time-slice at some arbitrary time. Figure 7 shows the flowfield near the injector tip. A finer grid system (101x15, and 301x141) was employed to simulate the RCM-1-B. The numerical results of RCM-1-B test case are plotted in Figures 8-12. The flowfield is presented in Fig. 13. Notice that only a small segment of the chamber is shown so that gradients in the flowfield may be clearly seen.

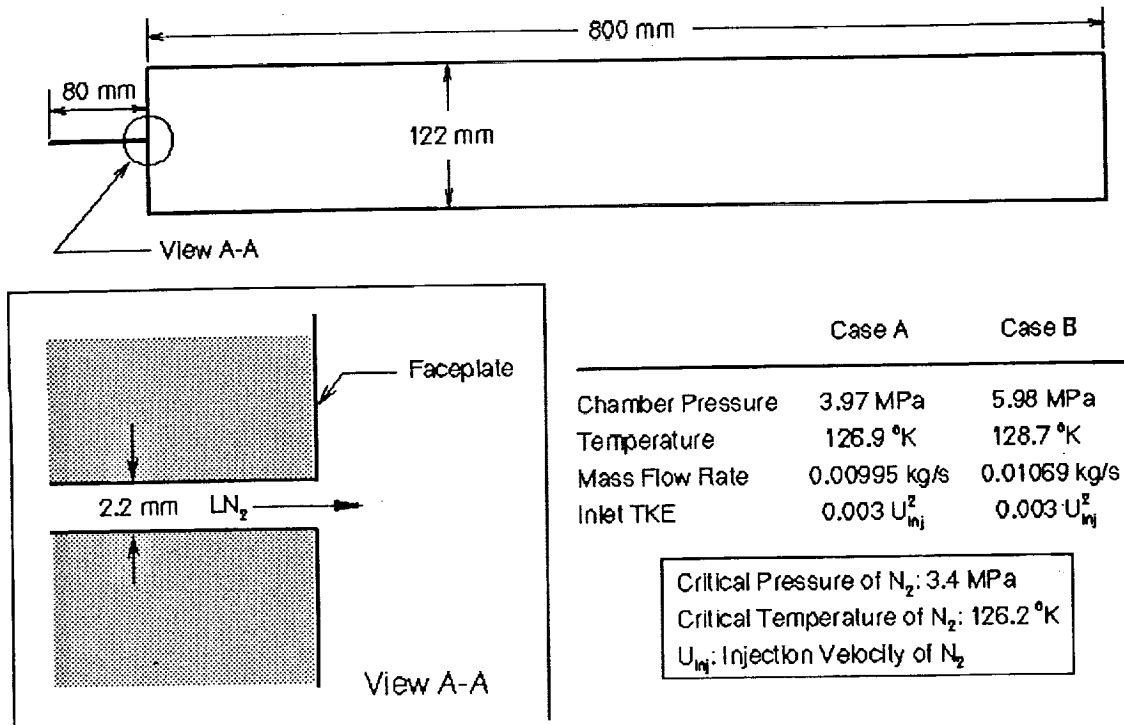


Figure 1 Configuration of RCM-1 Test Case

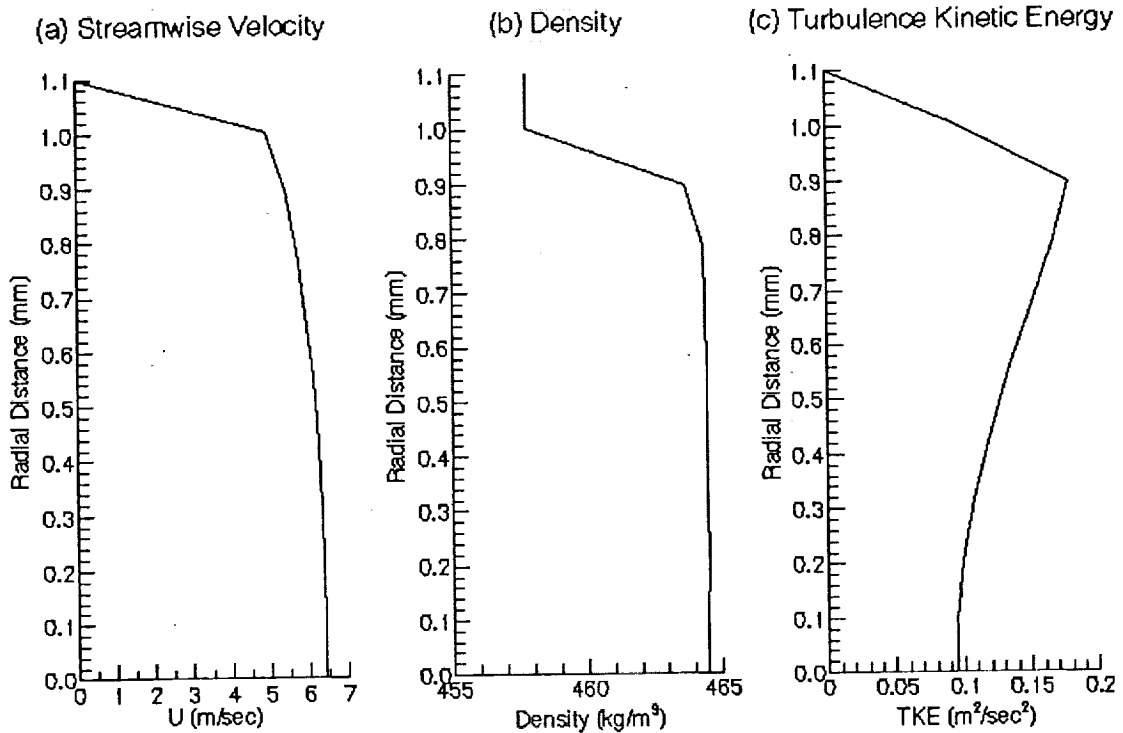


Figure 2 Flow Properties at the Injector Exit of RCM-1-A

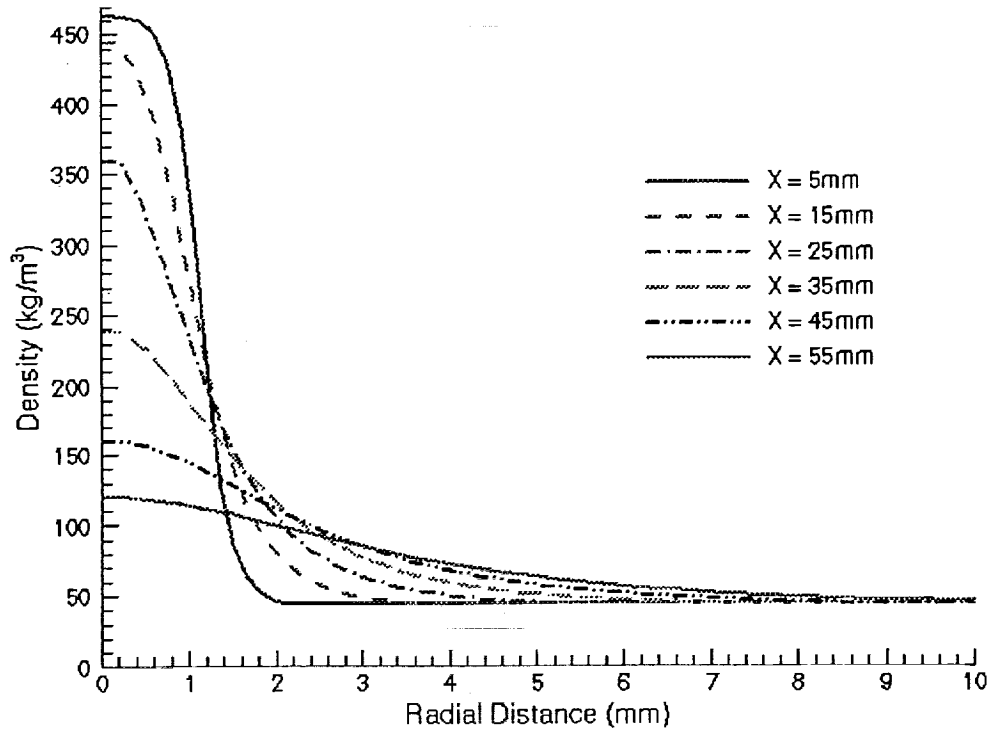


Figure 3 Density Profiles at Various Streamwise Locations of RCM-1-A

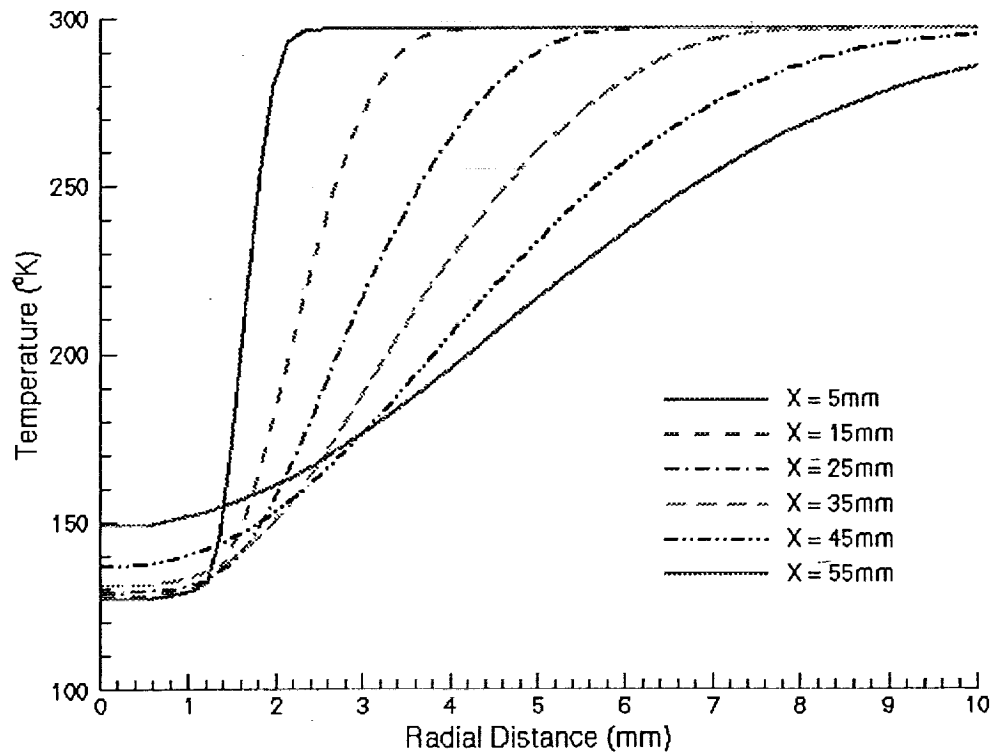


Figure 4 Temperature Profiles at Various Streamwise Locations of RCM-1-A

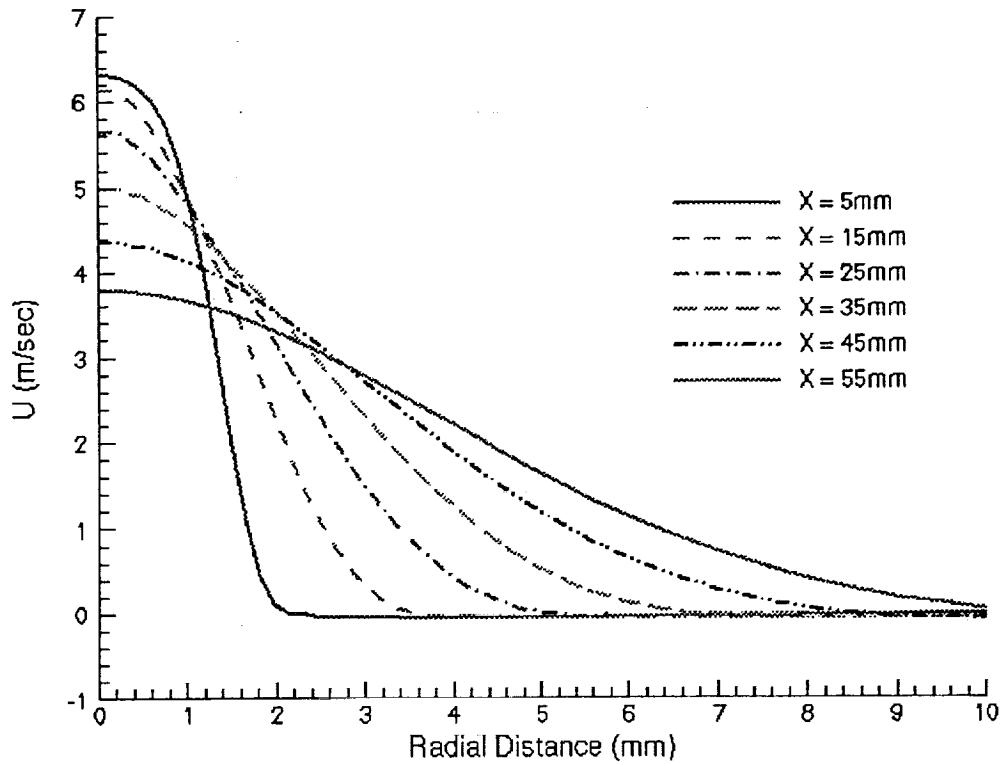


Figure 5 Axial Velocity Profiles at Various Streamwise Locations of RCM-1-A

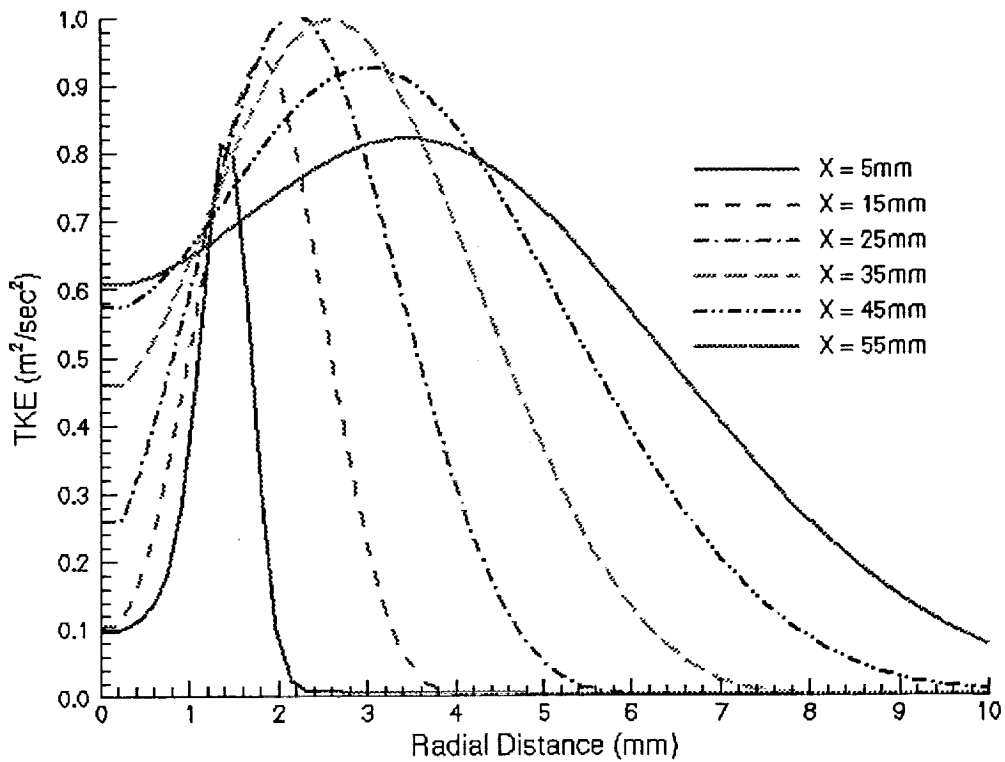


Figure 6 Turbulent Kinetic Energy Profiles at Various Streamwise Locations of RCM-1-A

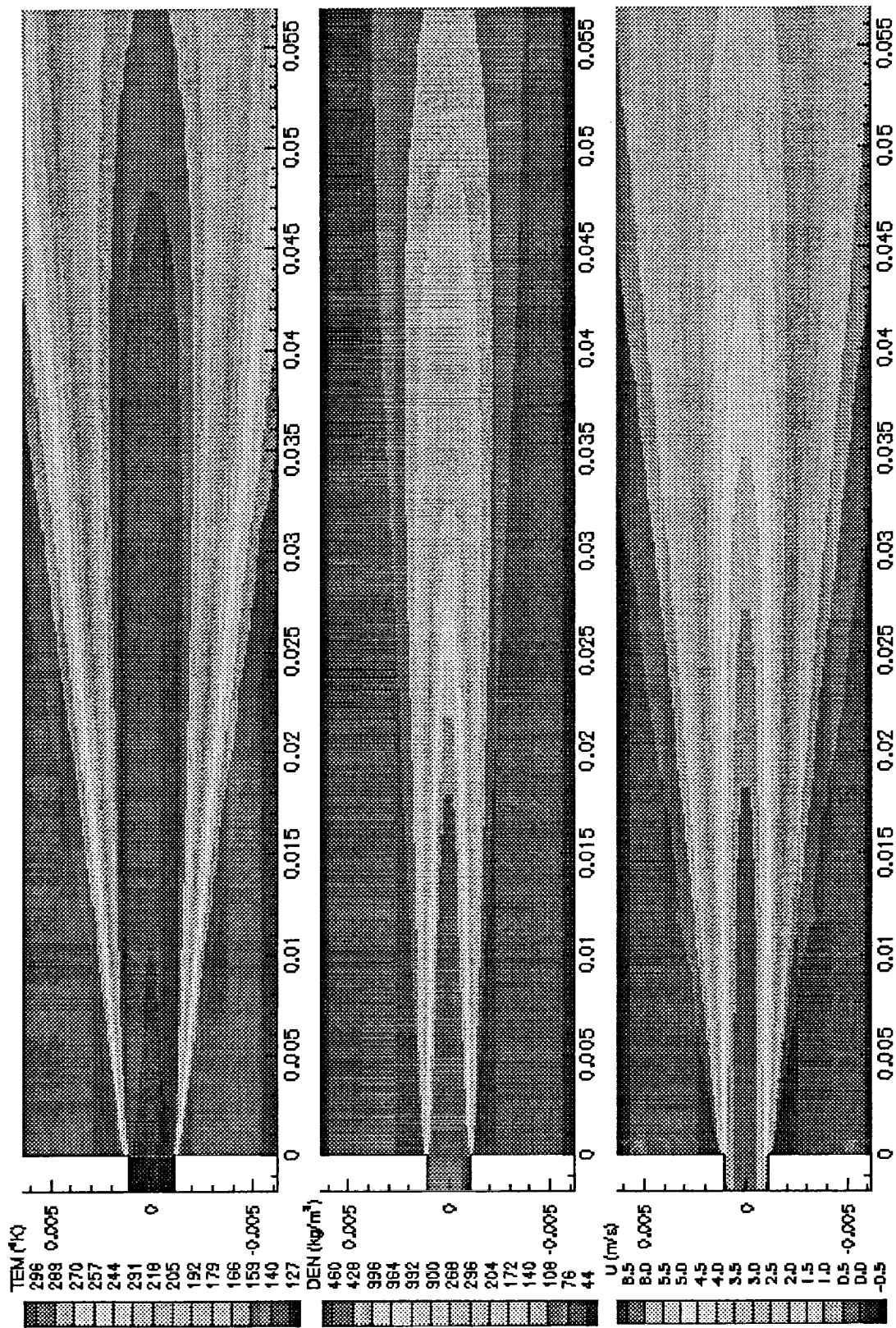


Figure 7 Flow Properties Near the Injector of RCM-1-A

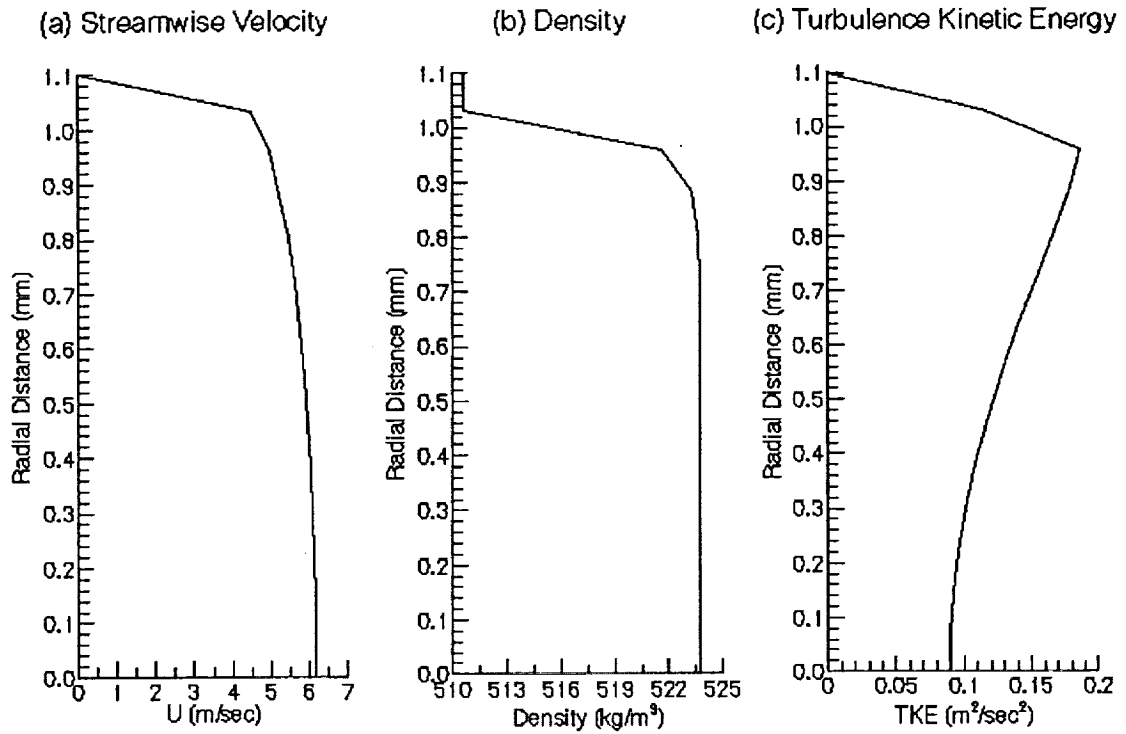


Figure 8 Flow Properties at the Injector Exit of RCM-1-B

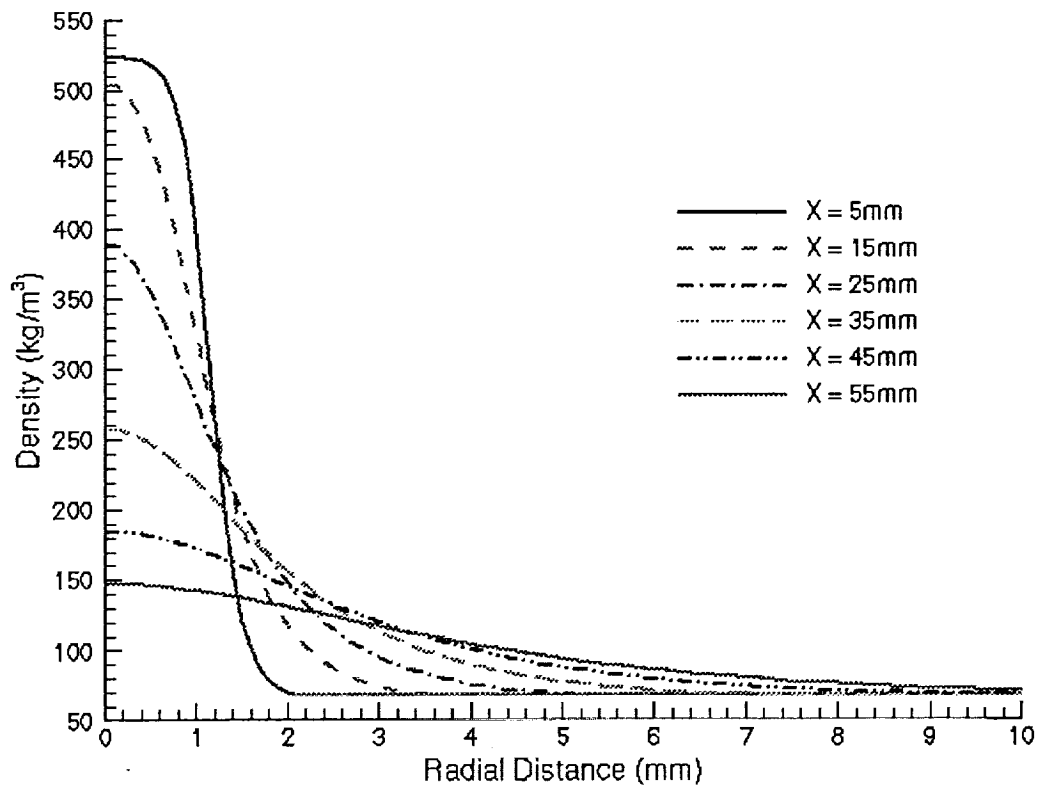


Figure 9 Density Profiles at Various Streamwise Locations of RCM-1-B

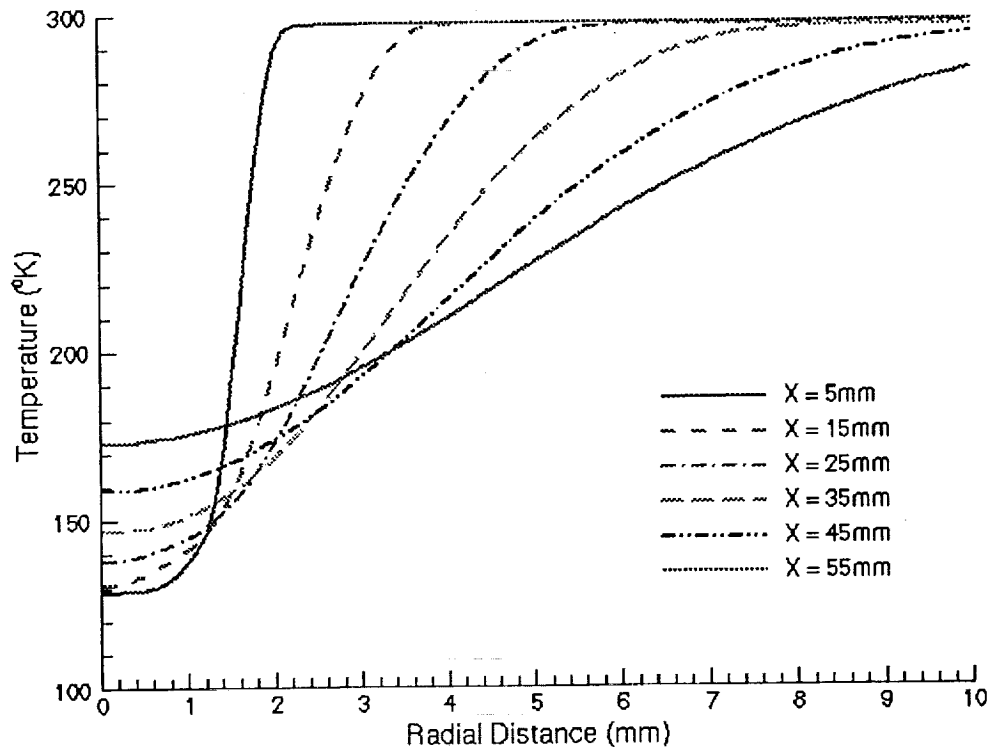


Figure 10 Temperature Profiles at Various Streamwise Locations of RCM-1-B

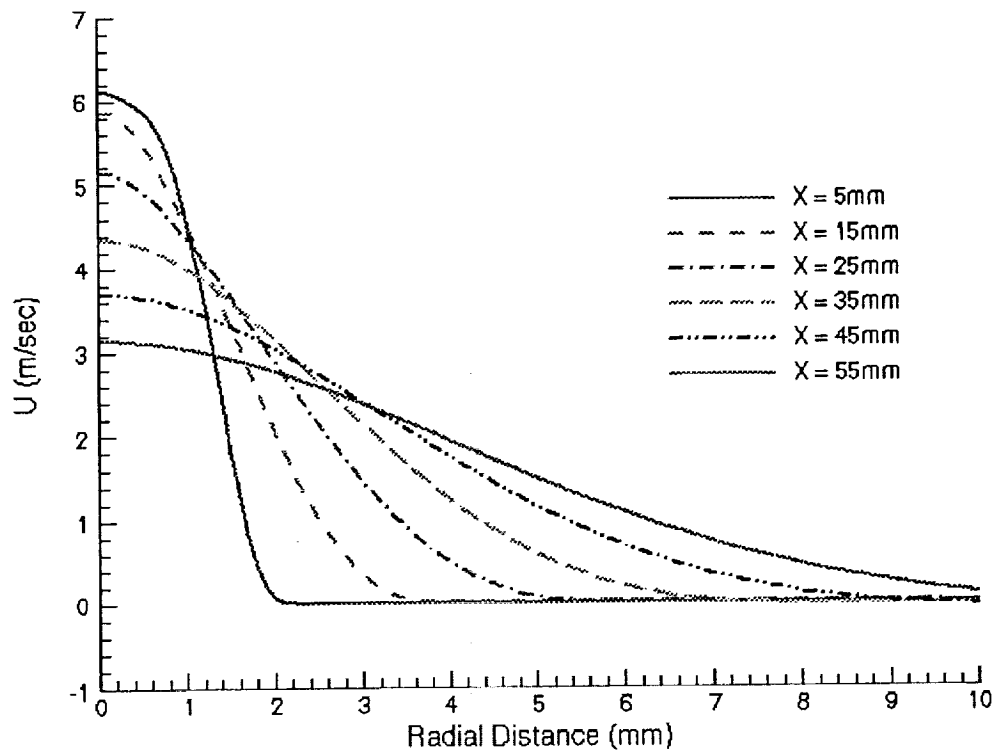


Figure 11 Axial Velocity Profiles at Various Streamwise Locations of RCM-1-B

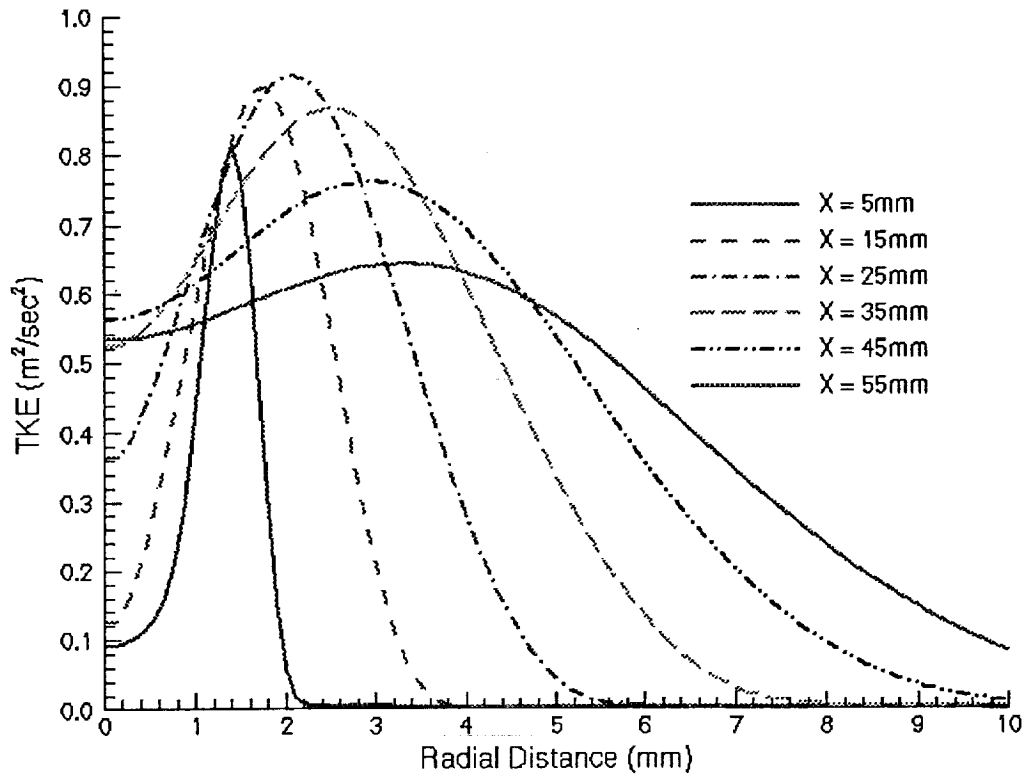


Figure 12 Turbulent Kinetic Energy Profiles at Various Streamwise Locations of RCM-1-B

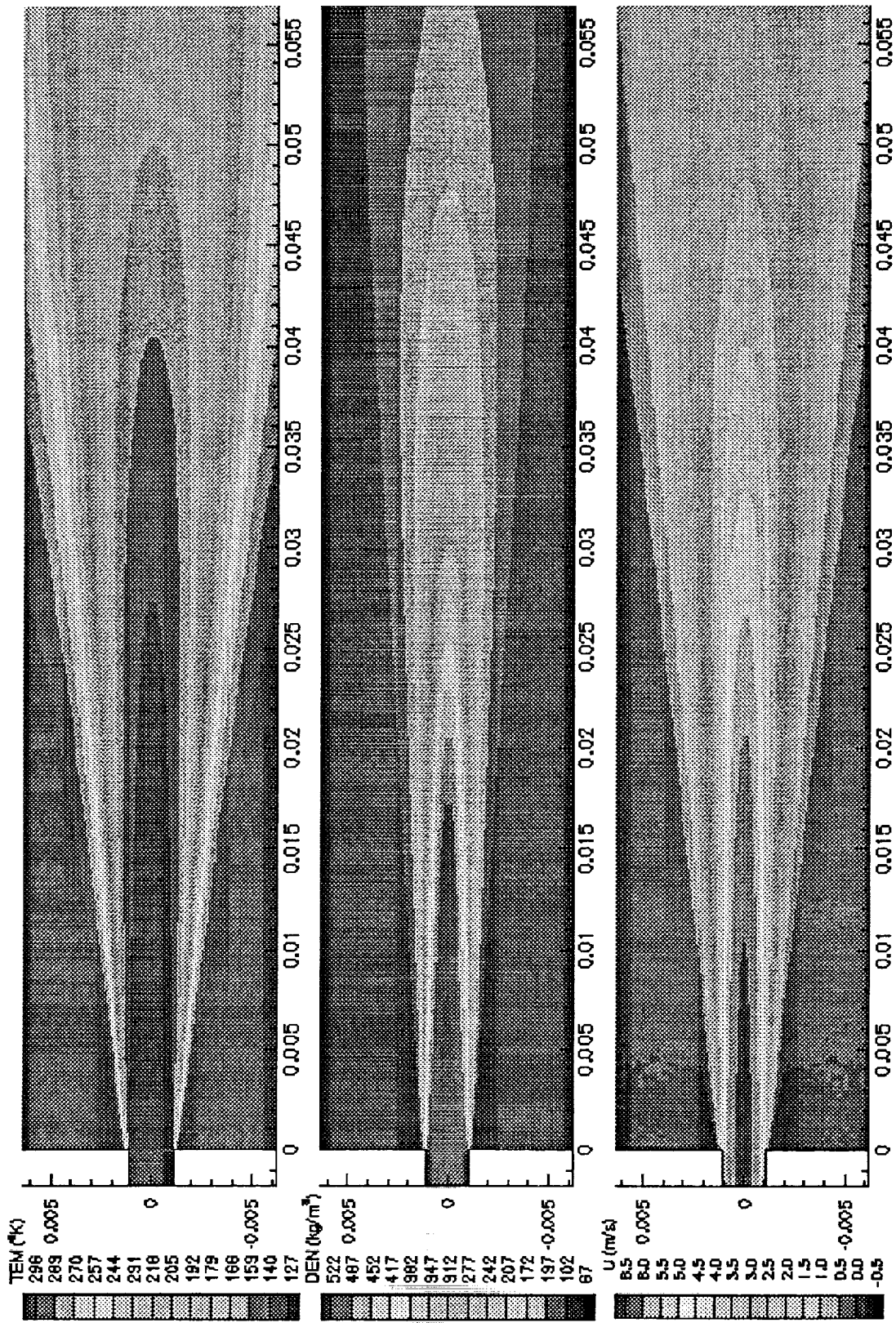


Figure 13 Flow Properties Near the Injector of RCM-1-B

SIMULATIONS OF THE RCM-2 EXPERIMENTS

The sub-critical combustion case, RCM-2, was simulated with both the heterogeneous and the homogeneous spray combustion models. The MASCOTTE test data should be better than any which have been previously used to tune the several parameters in these models. It is unreasonable to expect that spray flames, even of hydrogen and oxygen, can be accurately predicted without extensive model validation with test data representative of the conditions which exists in rocket engine combustion chambers. Even global data like chamber pressure and thrust have not been obtained for single coaxial element combustor flows. The IWRCM data provide a good starting point, but no CFD model tuning has yet been attempted for such experiments. Direct comparisons of predictions to test data at this point will not establish which of several modeling techniques is best.

The MASCOTTE single injector test chamber was used in a series of experimental programs for subcritical and/or supercritical H₂-O₂ combustion. In the subcritical spray combustion test case (RCM-2), the designed chamber pressure is 10 bar (or 9.87 atm). The injector orifice diameter for the liquid oxygen (LOX) injection is 5 mm surrounded by an annular gaseous hydrogen jet with channel width of 6.4 mm. The overall O/F ratio for this case is 2.11 (see the test conditions given in Table 2).

Table 2. RCM-2 Test Case Operating Conditions

Conditions	H ₂	O ₂
Pressure	1 MPa	1 MPa
Mass flow rate	23.7 g/s	50 g/s
Temperature	287 K	85 K
Density	0.84 kg/m ³	1170 kg/m ³
C _p	14300 J/kg/K	1690 J/kg/K
Velocity	319 m/s	2.18 m/s
Viscosity	8.6E-6 kg/m/s	1.94E-4 kg/m/s
Surface Tension	-	1.44E-2 N/m

The computational model includes the injector geometry, the combustion chamber and the nozzle section. A 10-block structured mesh is generated (the total number of grid points equals 14,444) for the two-phase flow computation. Relative high grid density (about 10 micron spacing) is packed in the injector lip region for the purpose of better flow resolution and flame holding in the expected area. The LOX core length of 7.8 mm is assumed, which serves as the particle injection boundary with the fixed particle size (82 microns), velocity (10 m/s) and angle distributions given in the problem specification. Fixed mass-flow boundary conditions are used at the inlet while all flow properties are extrapolated at the nozzle exit. Supersonic exit flow develops as part of the solution.

The computation starts with a cold flow with inlet and chamber pressure specified. The two-phase flow particle breakup and evaporation model models are activated from the beginning. The time step size of the time-marching solution method is 1 μsec. After 1000 time steps of cold flow run, a heat source is introduced in the lip region between and oxygen and hydrogen streams where a recirculation zone is established. At the same time, the finite-rate chemistry model is turned on to start the flame spreading throughout the chamber. The chamber pressure drops at the beginning until the flame fills up the entire chamber. Then, the pressure started to build up to the expected level

when the inlet and exit flows show satisfactory mass conservation condition. The calculated averaged chamber pressure is around 9.96 atm. The majority of the LOX particles do not survive very far downstream of the injector exit. Some particles along the chamber axis do survive up to 70 mm downstream of the injector.

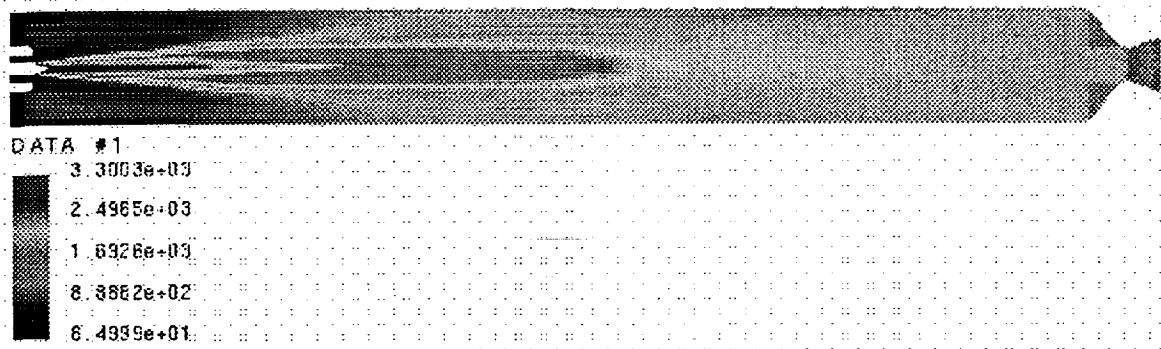
The time-averaged temperature, temperature standard deviation, species mass-fraction contours and temperature profiles at specified locations are plotted in the following figures. These data are prepared as requested for data comparison purpose.

Figure 14 shows the mean temperature and standard deviation through the entire length of the combustion chamber. A close up view of the nozzle tip region is also shown in this figure. Figure 15 shows the OH and O₂ and Figure 16 the H₂ and H₂O concentration profiles, respectively, in this same region. Figures 17-25 show radial temperature and standard deviation profiles at various axial locations. Figures 26-30 show the axial temperature profiles at various radial locations. Figure 30 shows this profile at the near wall location. The flame predicted with this model is long and narrow. The recirculation zone is very long.

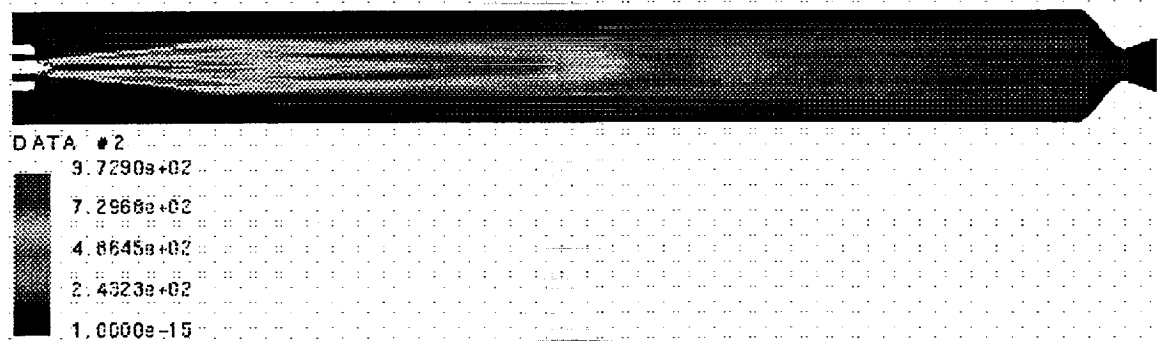
The RCM-2 experiment was also simulated with the homogeneous spray combustion model. The volume upstream of the injector element tip was neglected for this simulation. The grid use for the internal element flow was 61 X 43; for the chamber it was 301 X 101. The nozzle was not simulated. This grid system had a minimum grid spacing of 60 microns in the wake behind the lip separating the LOX and hydrogen streams. The boundary conditions used are shown in Figure 31. An equilibrium and several finite rate solutions were obtained for this configuration. The rate of the global initiation reaction was set fast enough to stabilize the flame near the start of the shear layer. This rate also essentially eliminated the waviness in the shear layer separating the LOX and hydrogen streams, without averaging the solution. The stoichiometric coefficients in the global rate expression were determined by an equilibrium calculation for a stoichiometric flame at the expected chamber pressure. Such a practice produces temperatures with one rate expression which are very close to those resulting from using a more detailed reaction mechanism.

The equilibrium solution at the interface between the internal element flow and the flow at the nozzle tip are shown in Figure 32. The temperature profiles in the radial and axial directions are shown in Figures 33 and 34, respectively. The temperature and oxygen and OH concentration profiles are shown in Figure 35. The wall temperature profile is shown in Figure 36. All of these figures are for the equilibrium solution. The finite rate solutions for the single global reaction and for the global plus the elementary reactions of Table 1 were also obtained. As expected, the finite rate solutions were slightly cooler than the equilibrium solutions. The predictions are very similar in all results to those just shown. To emphasize this point the wall temperature profiles for all three cases are shown in Figure 36. Even though the global rate was set fast enough to stabilize the flame with this grid system, it was not so fast that equilibrium conditions were obtained.

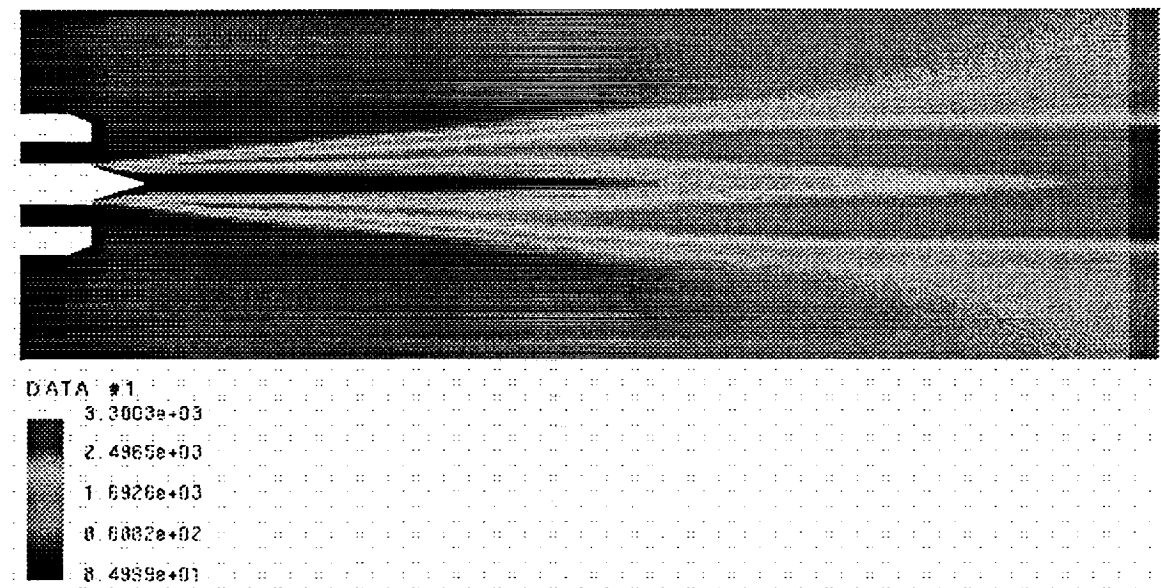
Comparing the heterogeneous and homogeneous solutions, the former produced a longer, thinner flame than the latter. Parameters in the spray combustion model could have been set such that the solutions matched very closely, or so that both could match test data. Such a step cannot be made until the RCM test data are published and the CFD models tuned. An optimum rocket engine spray combustion model cannot be determined until this next validation step is undertaken.



(a) Time-Averaged Temperature (K)

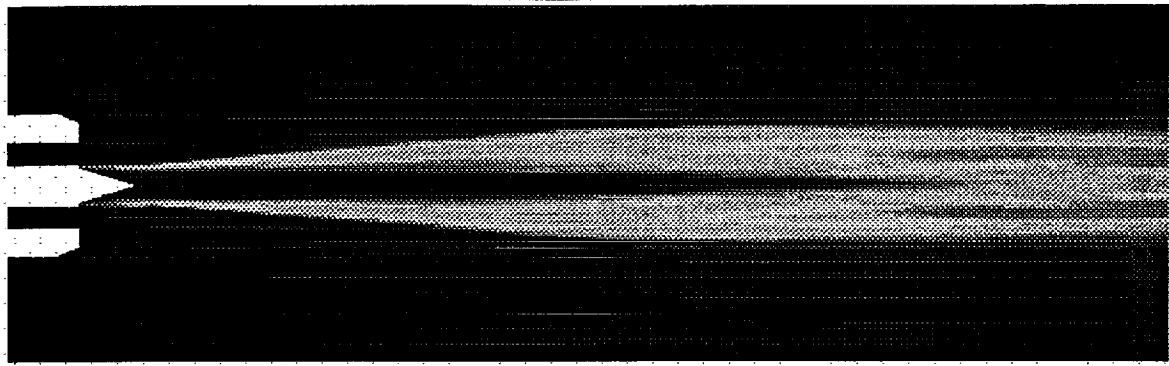


(b) Temperature Standard Deviation (K)



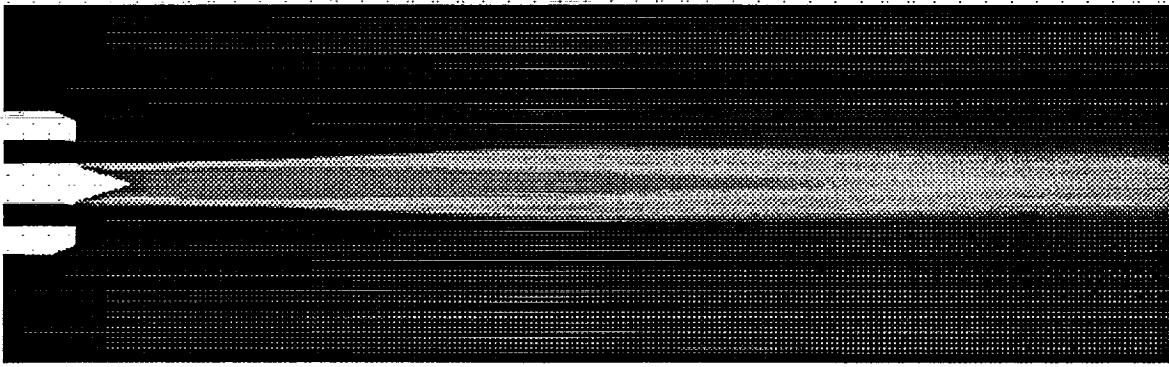
(c) Time-Averaged Temperature (K) for X up to 150 mm

Figure 14 Time-Averaged Temperature and Temperature Standard Deviation of RCM-2



DATA #5
 1.0120e-01
 7.5903e-02
 5.0802e-02
 2.5301e-02
 1.0000e-30

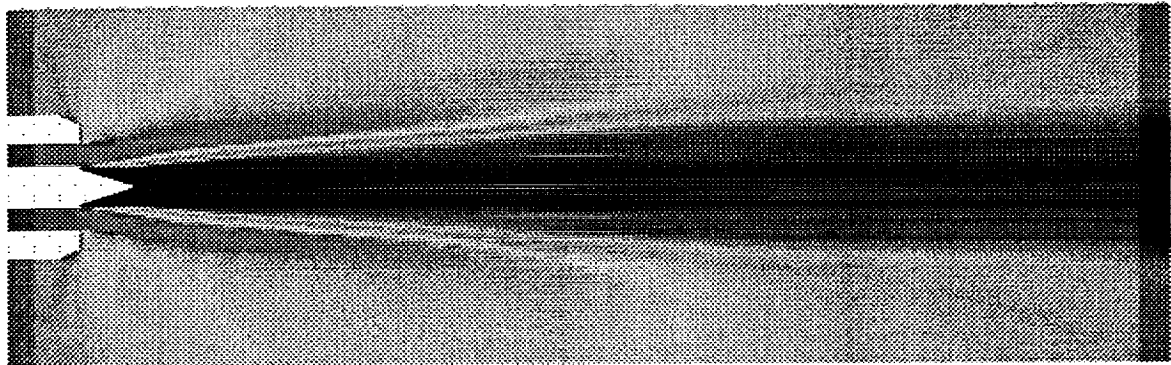
(a) Time-Averaged OH Mass-Fraction Contours for X up to 150 mm



DATA #5
 9.9999e-01
 7.4999e-01
 5.0000e-01
 2.5000e-01
 2.1288e-22

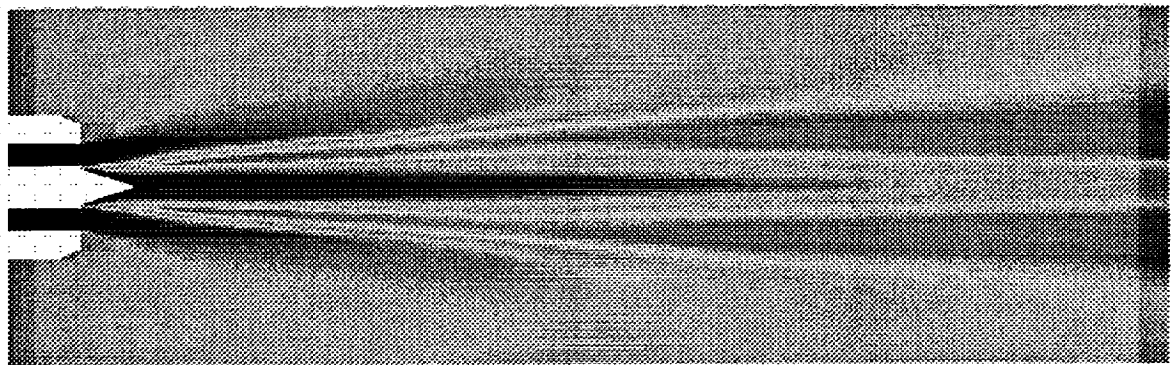
(b) Time-Averaged O₂ Mass-Fraction Contours for X up to 150 mm

Figure 15 Time-Averaged OH and O₂ Mass Fractions of RCM-2



DATA #1
 9.9999e-01
 7.4999e-01
 5.0000e-01
 2.5000e-01
 1.0000e-30

(a) Time-Averaged H₂ Mass-Fraction Contours for X up to 150 mm



DATA #2
 0.6435e-01
 6.4828e-01
 4.3217e-01
 2.1609e-01
 1.0000e-30

(b) Time-Averaged H₂O Mass-Fraction Contours for X up to 150 mm

Figure 16 Time-Averaged H₂ and H₂O Mass Fractions of RCM-2

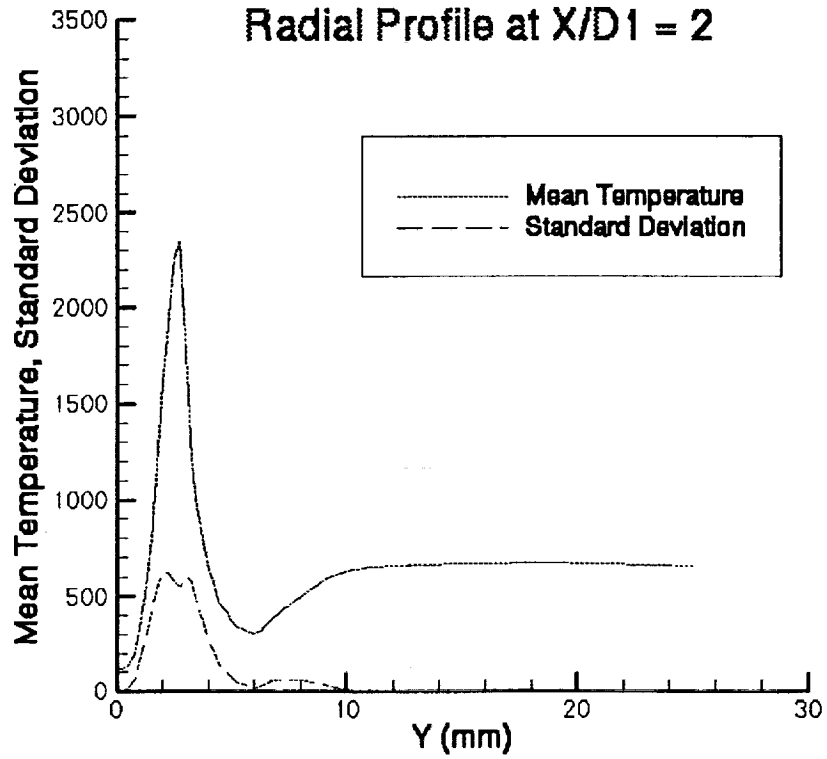


Figure 17 Radial Profiles of Mean Temperature and Standard Deviation at X/D = 2 of RCM-2

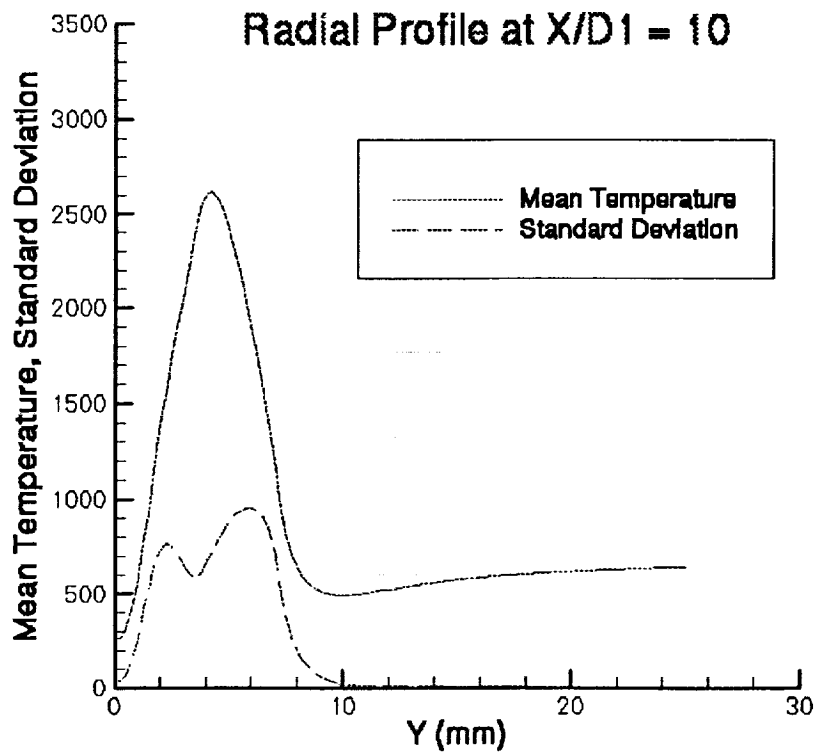


Figure 18 Radial Profiles of Mean Temperature and Standard Deviation at X/D = 10 of RCM-2

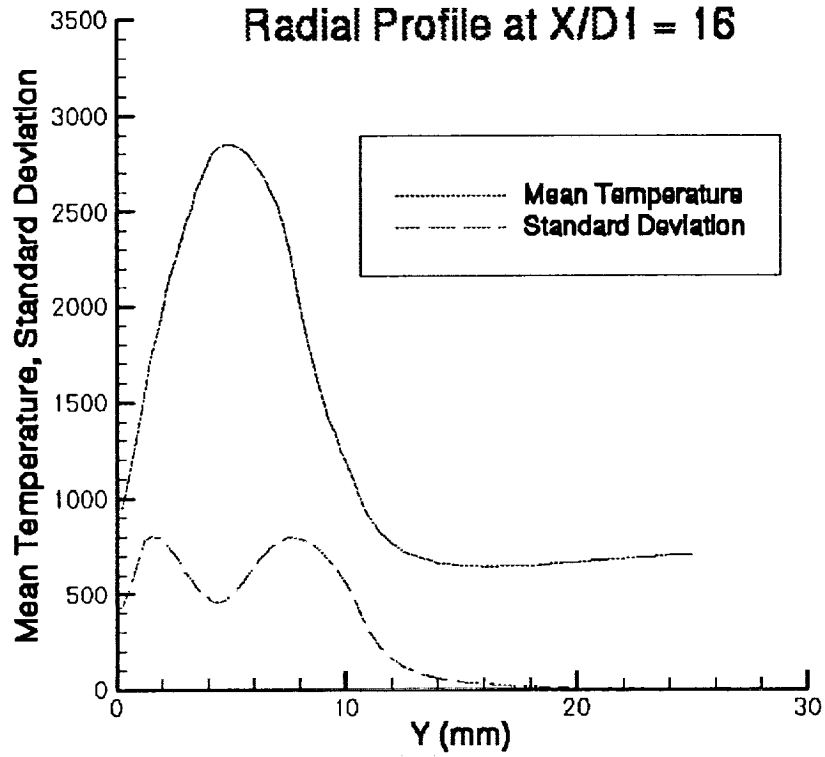


Figure 19 Radial Profiles of Mean Temperature and Standard Deviation at X/D = 16 of RCM-2

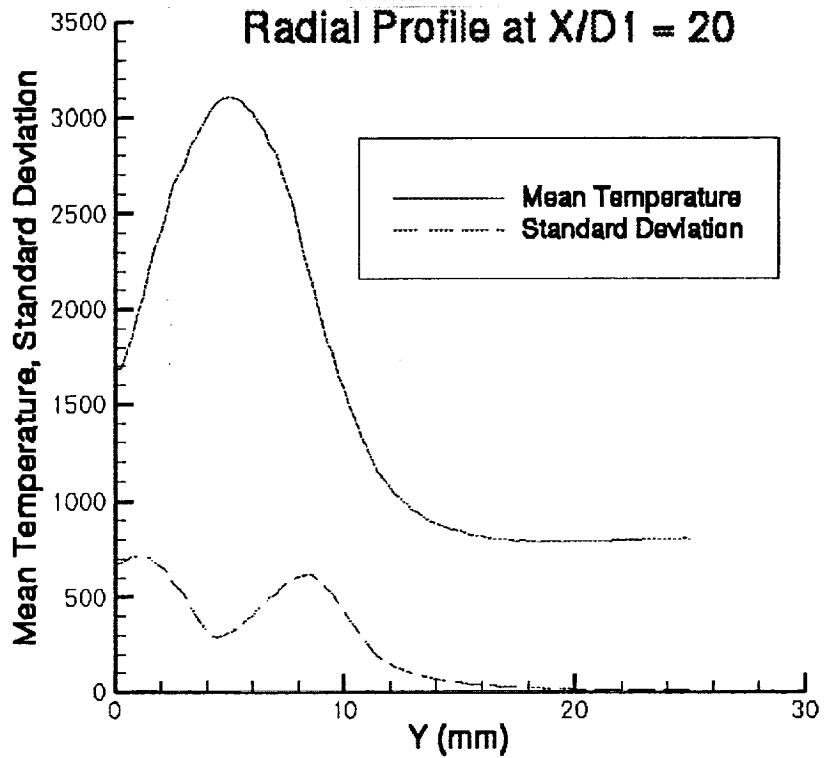


Figure 20 Radial Profiles of Mean Temperature and Standard Deviation at X/D = 20 of RCM-2

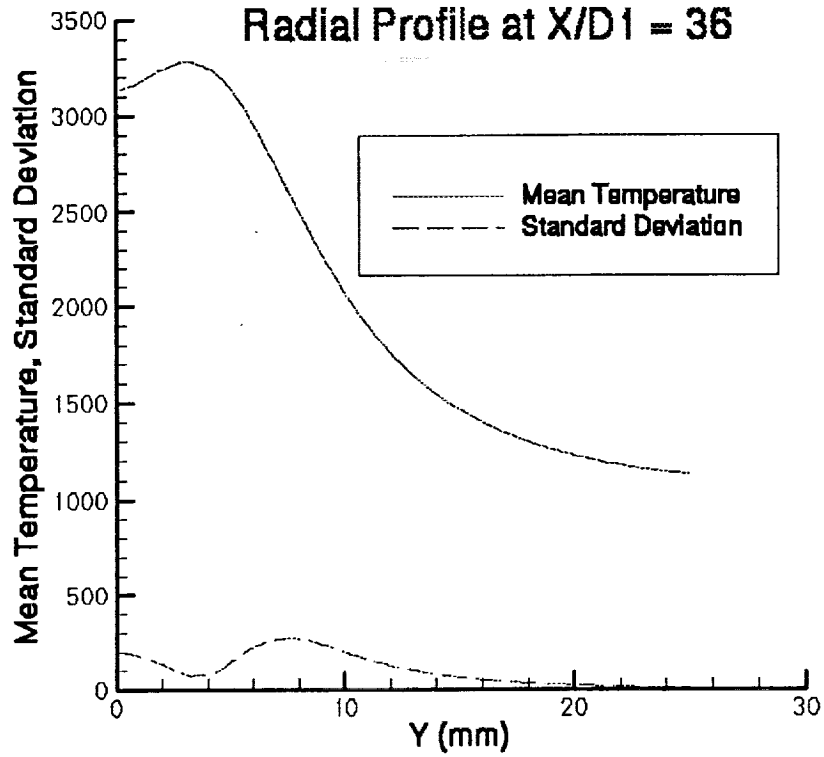


Figure 21 Radial Profiles of Mean Temperature and Standard Deviation at X/D = 36 of RCM-2

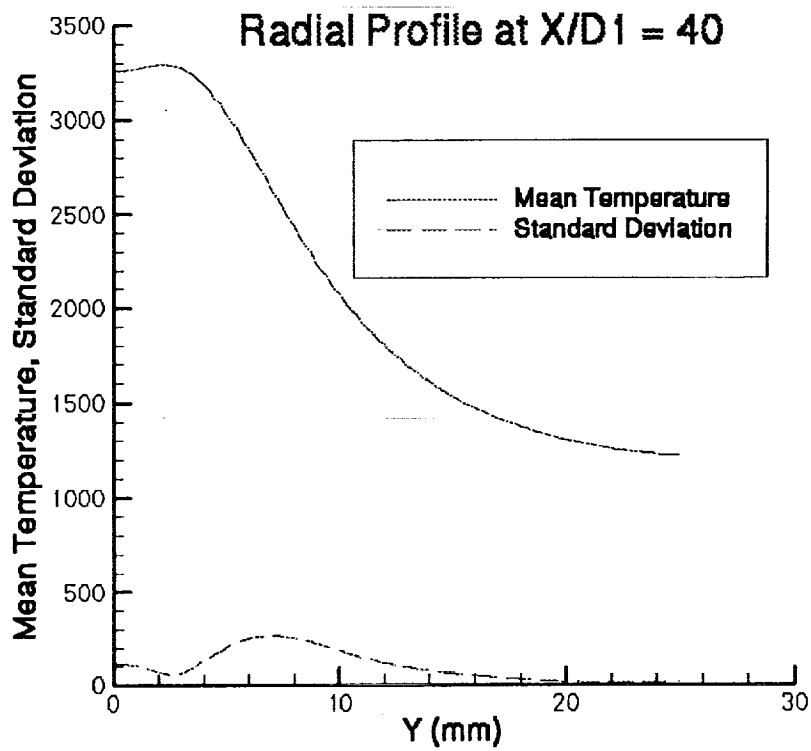


Figure 22 Radial Profiles of Mean Temperature and Standard Deviation at X/D = 40 of RCM-2

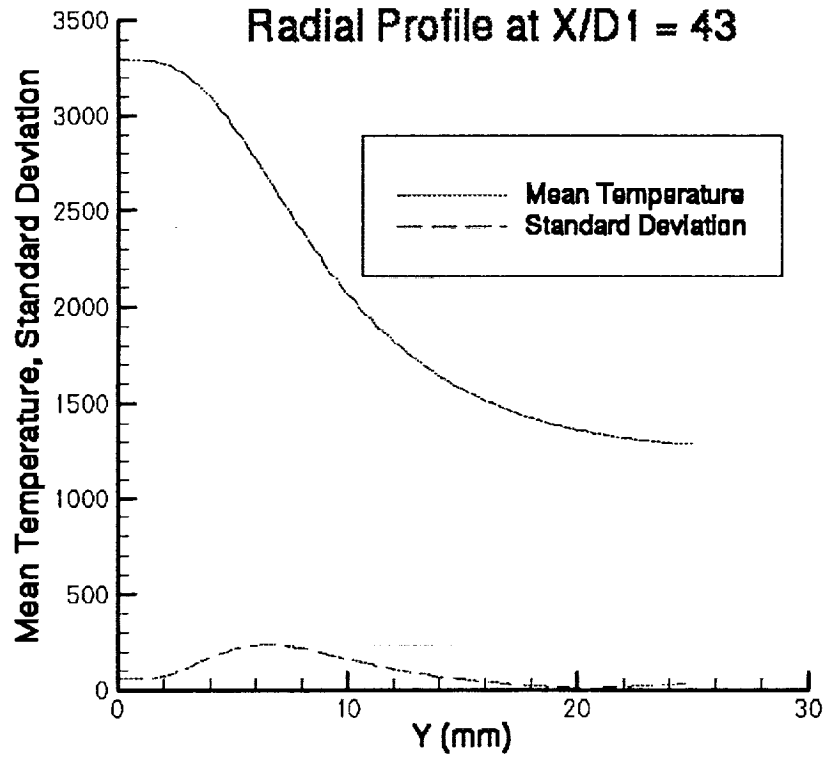


Figure 23 Radial Profiles of Mean Temperature and Standard Deviation at X/D = 43 of RCM-2

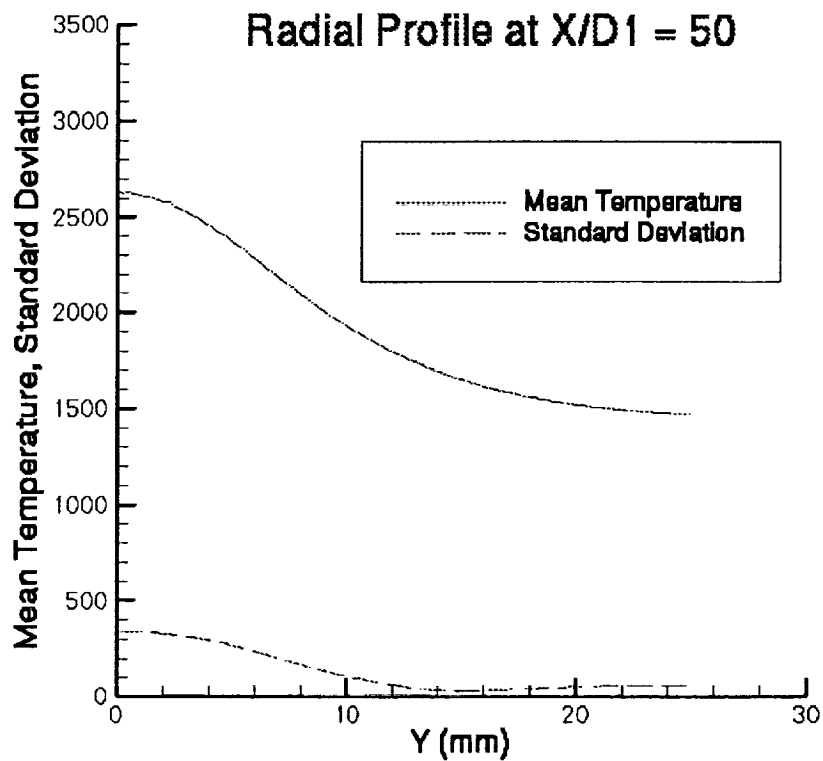


Figure 24 Radial Profiles of Mean Temperature and Standard Deviation at X/D = 50 of RCM-2

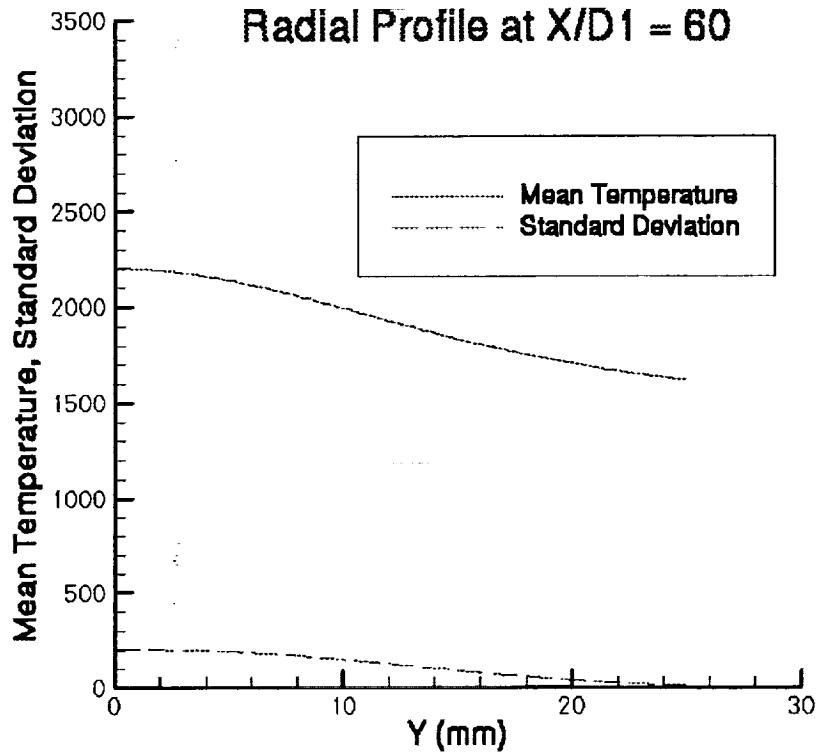


Figure 25 Radial Profiles of Mean Temperature and Standard Deviation at X/D = 60 of RCM-2

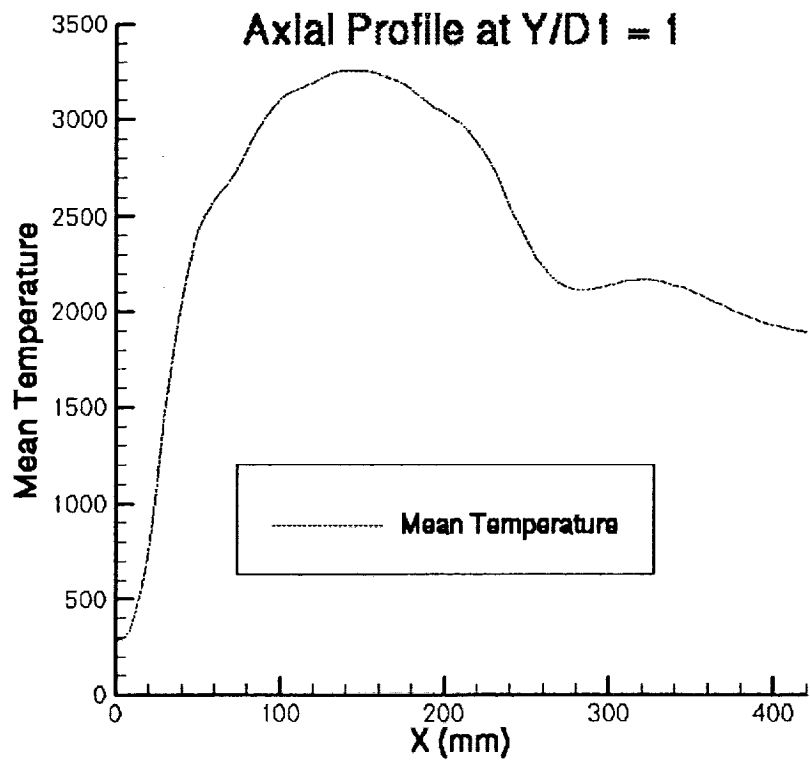


Figure 26 Axial Profiles of the Mean Temperature at Y/D = 1 of RCM-2

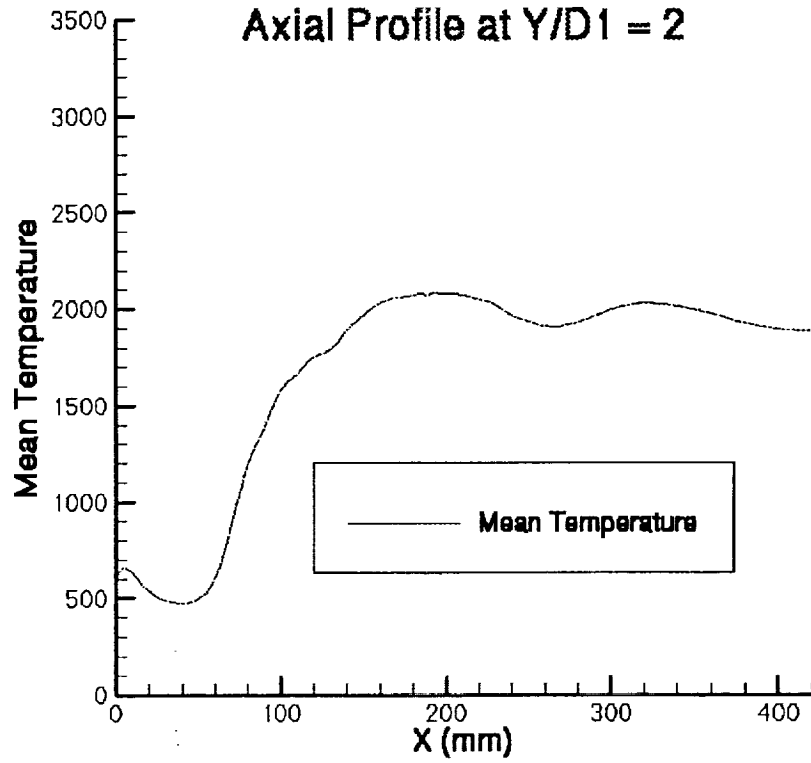


Figure 27 Axial Profiles of the Mean Temperature at Y/D = 2 of RCM-2

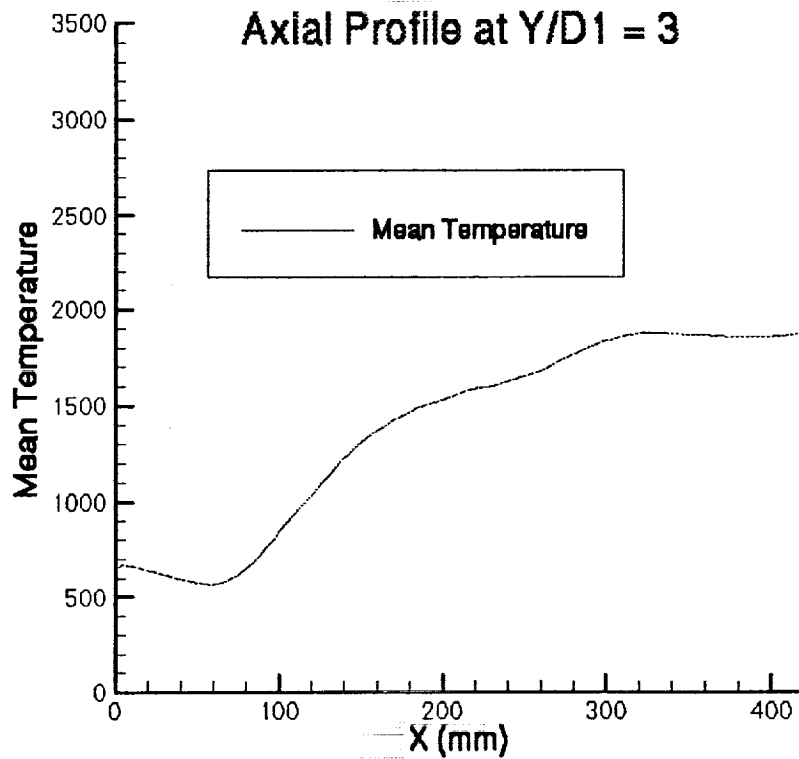


Figure 28 Axial Profiles of the Mean Temperature at Y/D = 3 of RCM-2

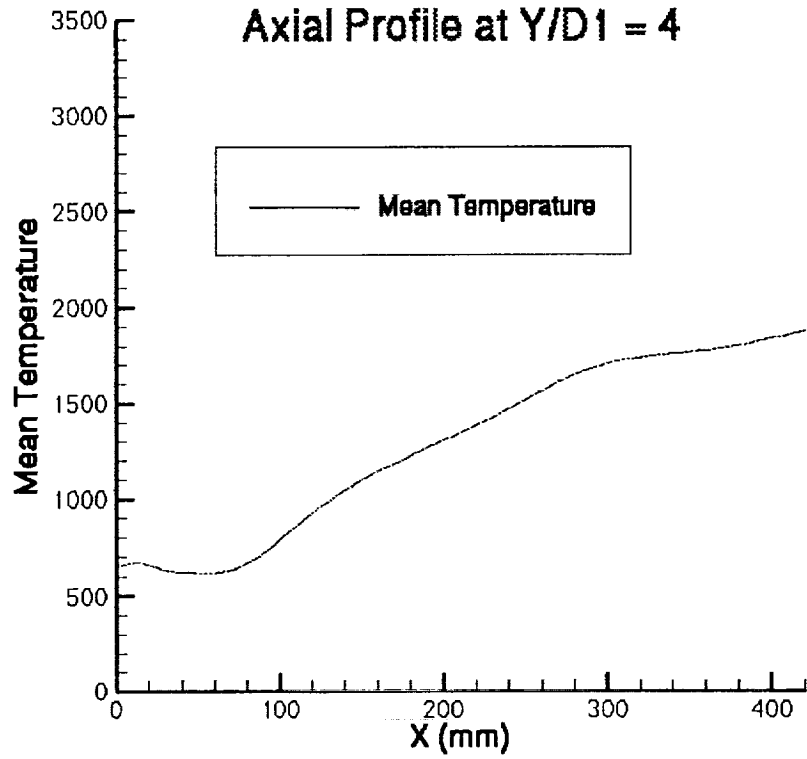


Figure 29 Axial Profiles of the Mean Temperature at Y/D = 4 of RCM-2

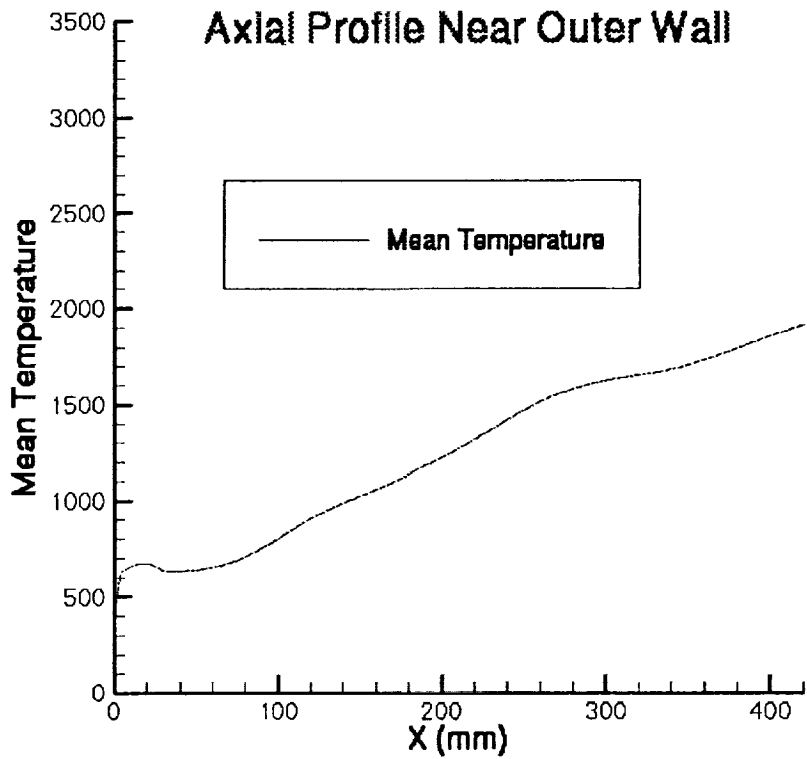


Figure 30 Axial Profiles of the Mean Temperature Near the Outer Wall of RCM-2

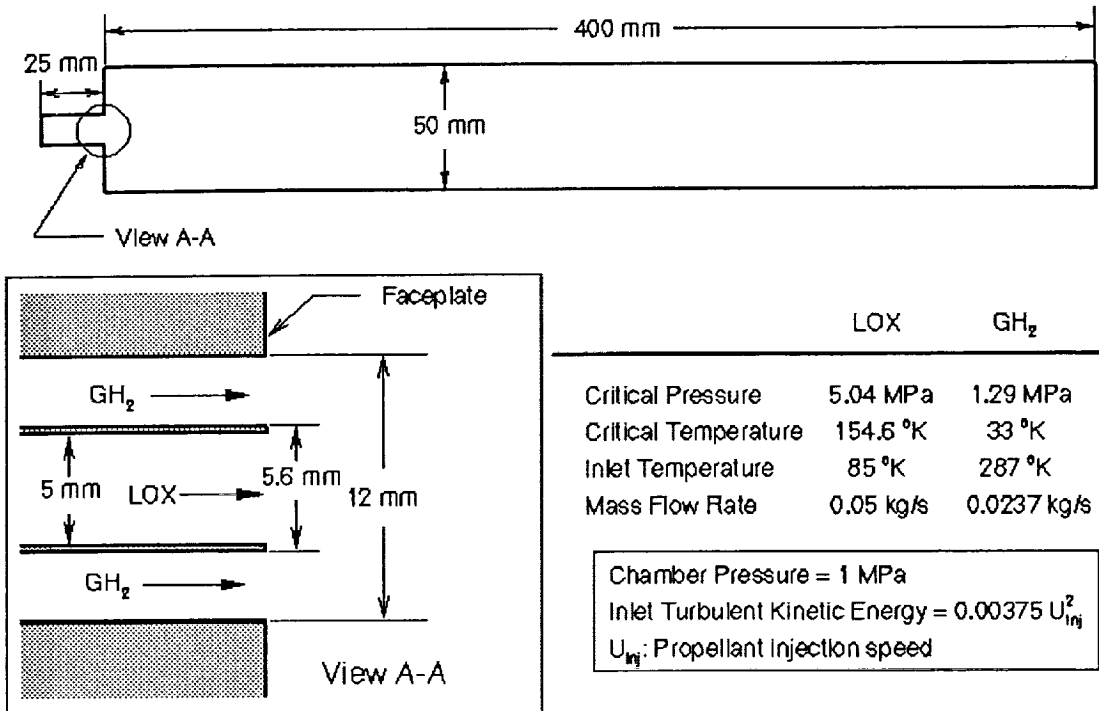


Figure 31 Configuration of the RCM-2 Case (Homogeneous Spray Model)

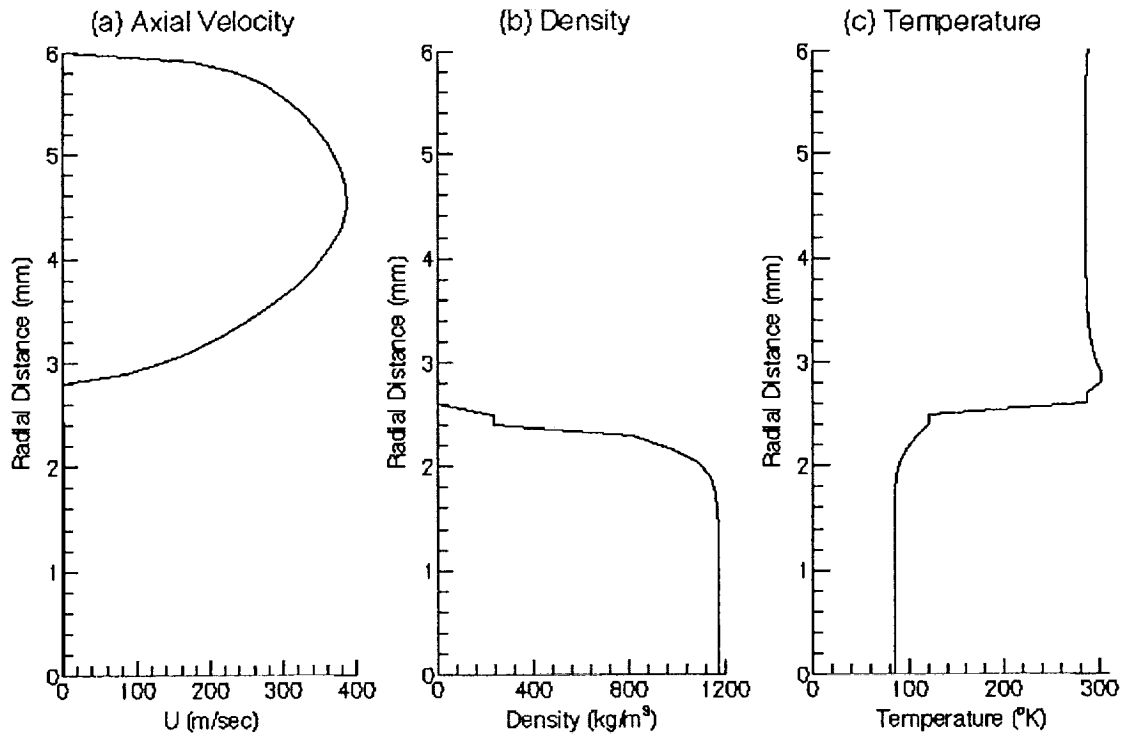


Figure 32 Flow Properties at the Injector Exit of RCM-2 (Homogeneous Spray Model)

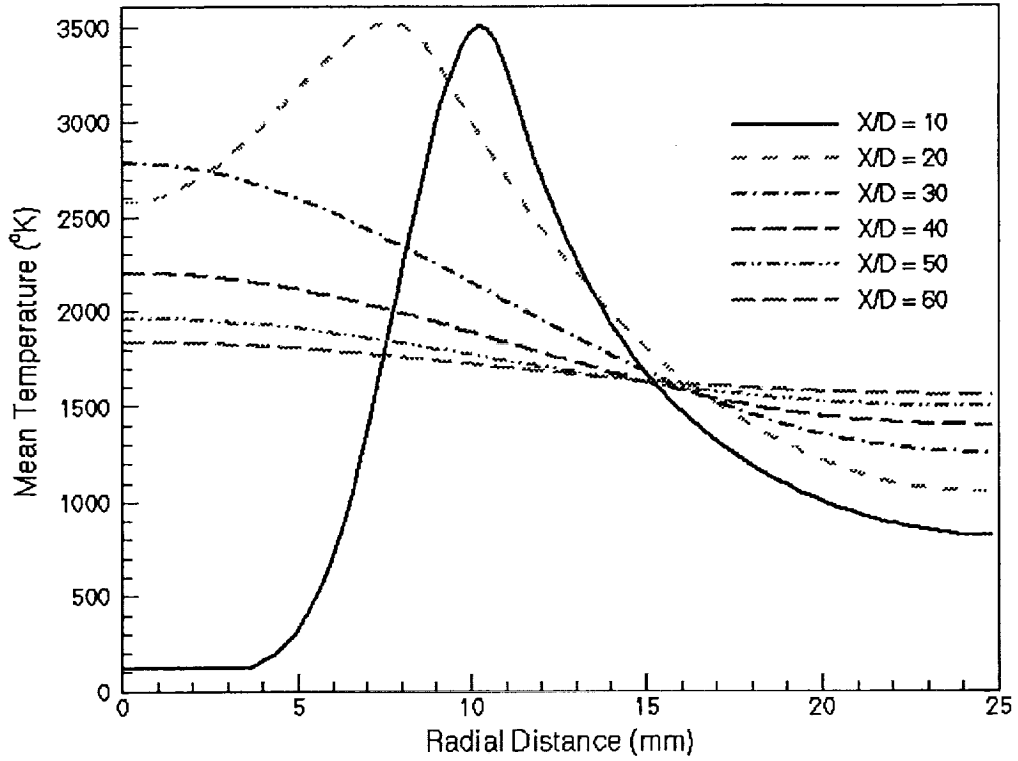


Figure 33 Radial Profiles of the Mean Temperature at Various Axial Locations of RCM-2

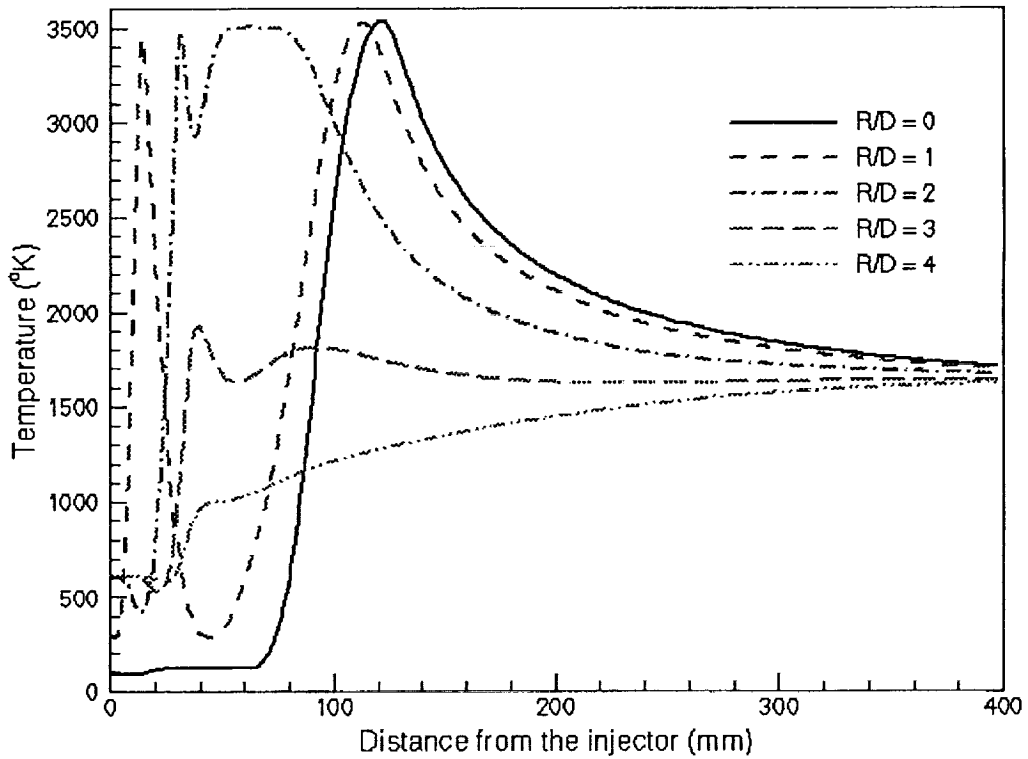


Figure 34 Axial Profiles of the Mean Temperature at Various Radial Locations of RCM-2

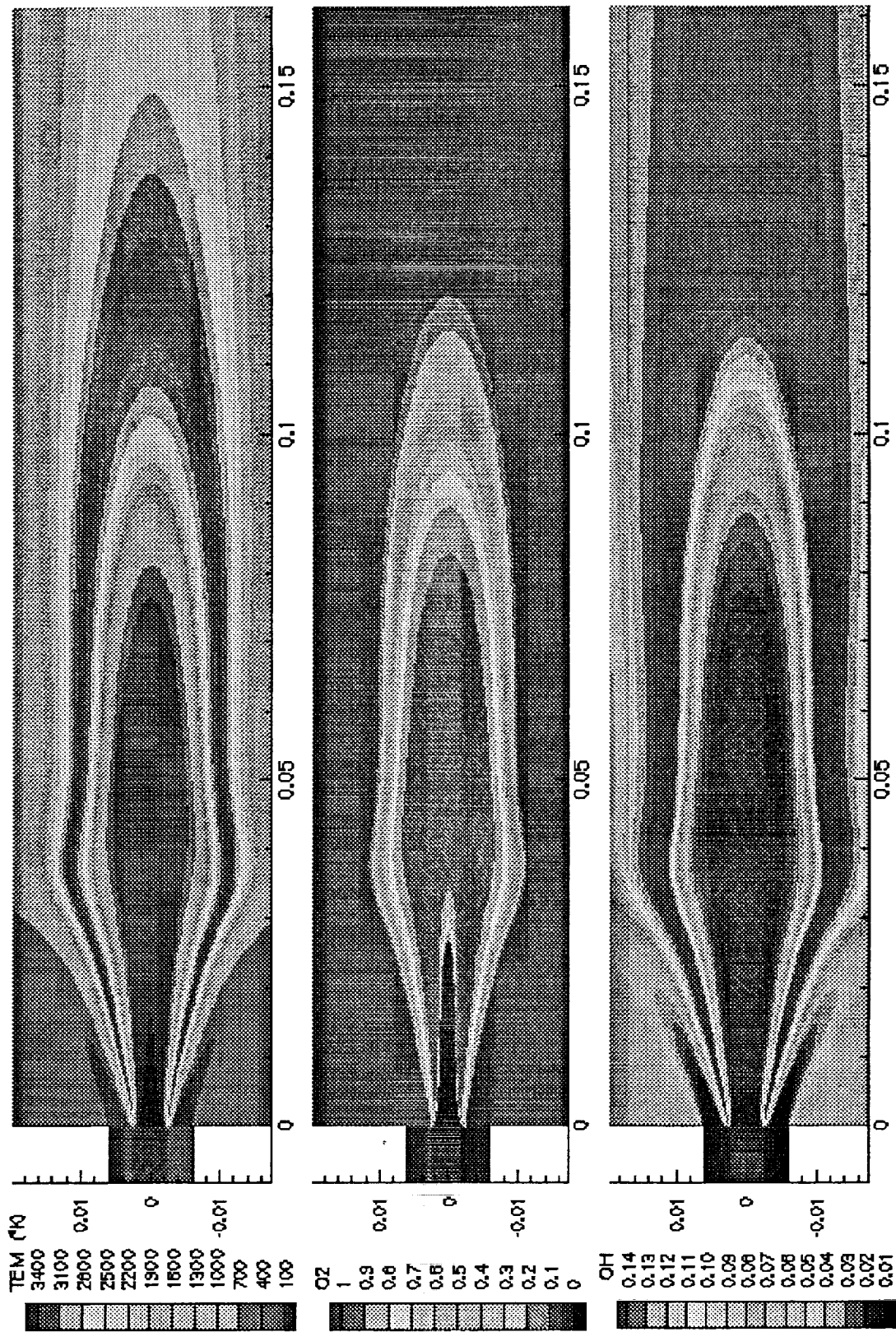


Figure 35 Temperature and Species Concentrations Near the Injector of RCM-2

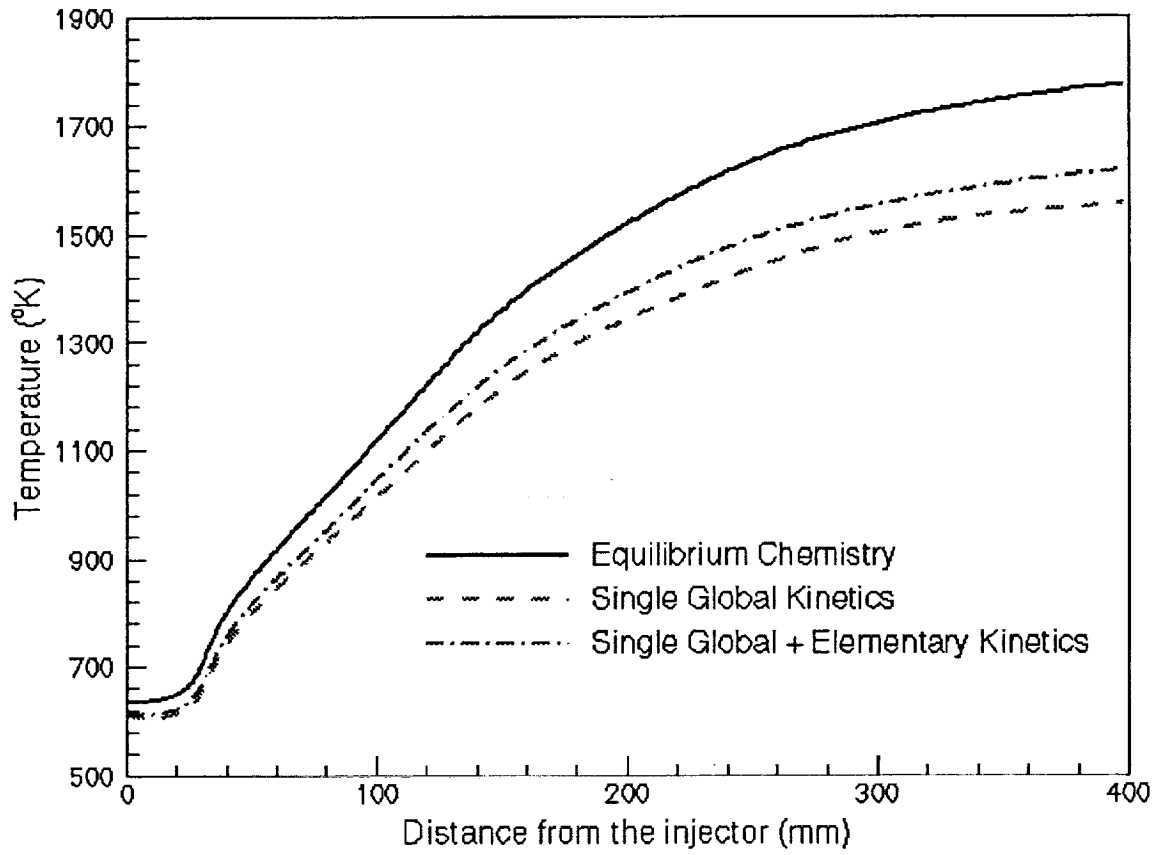


Figure 36 Near Wall Temperature Distributions for Various Chemistry Models of RCM-2

SIMULATIONS OF THE RCM-3 EXPERIMENT

The super-critical combustion case, RCM-3, was simulated with the homogeneous spray combustion model. Any drops present will be highly unstable; therefore, this model should represent the flow rather well. Local equilibrium and simplified finite-rate combustion submodels were used and the results for the two simulations compared well. More detailed combustion submodels were attempted, but proved to behave too poorly for successful simulations.

The preponderance of super-critical spray combustion models which have been reported have been extensions of sub-critical models. Such models encounter a basic problem in over emphasizing the role of surface tension. Since surface tension is zero for super-critical conditions, drops should not exist. Although such drops can be observed experimentally, they are extremely unstable and do not survive very long. The homogeneous CFD model was developed to account for the major physical effects which do exist. Namely, the large density and momentum differences which exist in multi-phase super-critical flows. Such a model allows one to accurately relate the inlet conditions at the injector face to boundary conditions for the CFD simulation. This relationship is essential to predicting the effects of injector element configuration and inlet momentum vector on the convective mixing and cross winds which occur in practical rocket engines. Otherwise, one is forced to use the historical method of creating costly experimental data bases from which to choose designs.

The injector configuration and flow conditions for the supercritical combustion of the RCM-3 test case are presented in Fig. 37. This is uni-element shear coaxial injector with LOX and GH_2 propellants. The numerical simulation was conducted with some simplification because, initially, detailed information was unavailable; such as: (1) the flare of LOX injector near the exit was neglected; (2) the injector was flush at the chamber head-end instead of protruding into the chamber because the outer diameter of hydrogen tube and distance between the chamber head-end and the injector exit were not known; (3) the nozzle was not included because of insufficient information about the chamber tail-end and nozzle geometry; and (4) the coolant (later found to be helium) for the chamber wall was not included because its flow rate and properties were not specified. As can be seen, the chamber pressure (60 bar) is well above the critical pressure of oxygen; hence, the homogeneous real-fluid model was used to simulate this test case. A two-zone mesh system (61x39 and 301x101) was used to model the injector section and the combustion chamber.

The combustion reactions in this high pressure experiment are expected to be in local thermodynamic equilibrium and were simulated as such. To demonstrate the methodology, two finite-rate simulations were also made with a subset of the reactions in Table 1. The single global reaction which produces radicals as well as water provides a good estimate of the temperature field. Its rate was set to attach the flame near the injector tip. Since the radicals are not rigorously simulated with the single reaction, a second finite-rate simulation was made with the 2-body reactions. Backward reaction rates are determined with equilibrium constants. For high pressure cases such combustion modeling is essential to keep the computation stable.

The chemistry and turbulence models used in our simulations do not make use of probability density functions (PDFs) because most of the shear layers formed by the injector element should be continuum. The only regions for which this might not be the case are the intermittent edges of the

shear layers. Pope⁸ terms these regions the "viscous superlayer". The thickness of these layers are inversely proportional to the Reynolds number to the 0.75 power. For these high speed coaxial jets, they should be very thin.

The flow predicted at the injector tip is shown in Figure 38. The radial temperature profiles predicted at several axial stations are shown in Figure 39. The axial profiles at several radial locations are shown in Figure 40. The temperature and oxygen and OH concentration profile fields are shown in Figure 41. The combustion models used do not predict chemiluminescent OH, which might be observed in the experiments. These results are shown for the equilibrium combustion model. Results for the two finite-rate combustion simulations are very similar, hence they are not shown. The wall temperature distributions for all three cases are compared in Figure 42, and as noted the results are very similar.

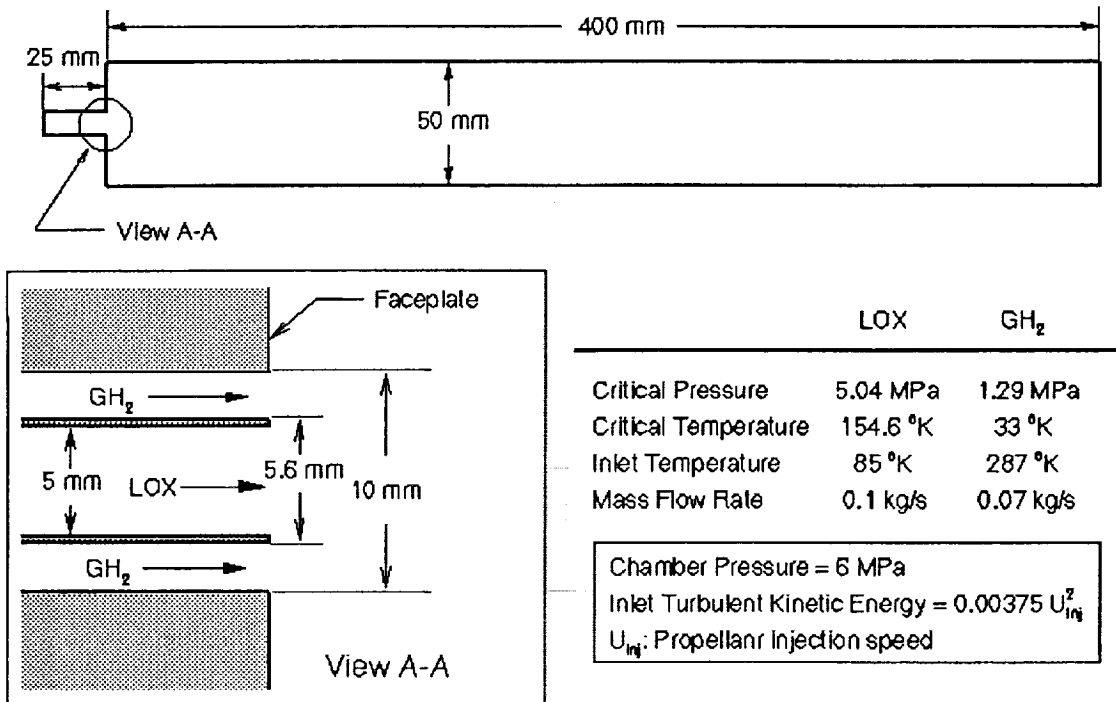


Figure 37 Configuration of the RCM-3 Case (Homogeneous Spray Model)

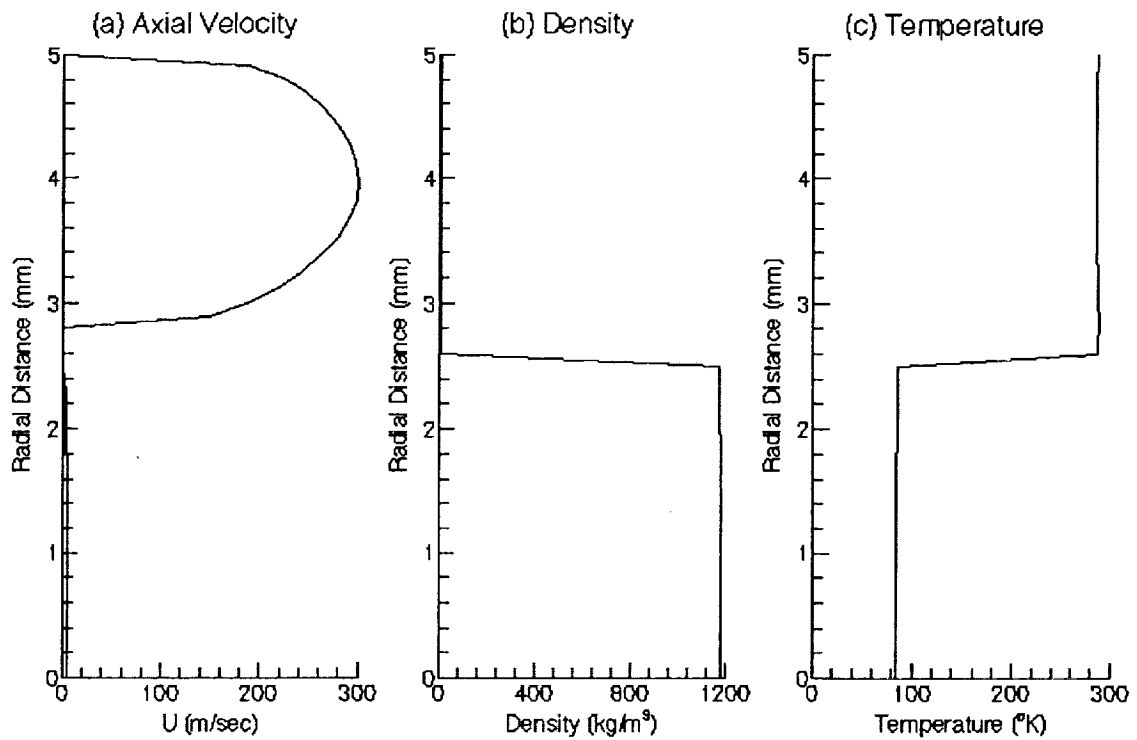


Figure 38 Flow Properties at the Injector Exit of RCM-3 (Homogeneous Spray Model)

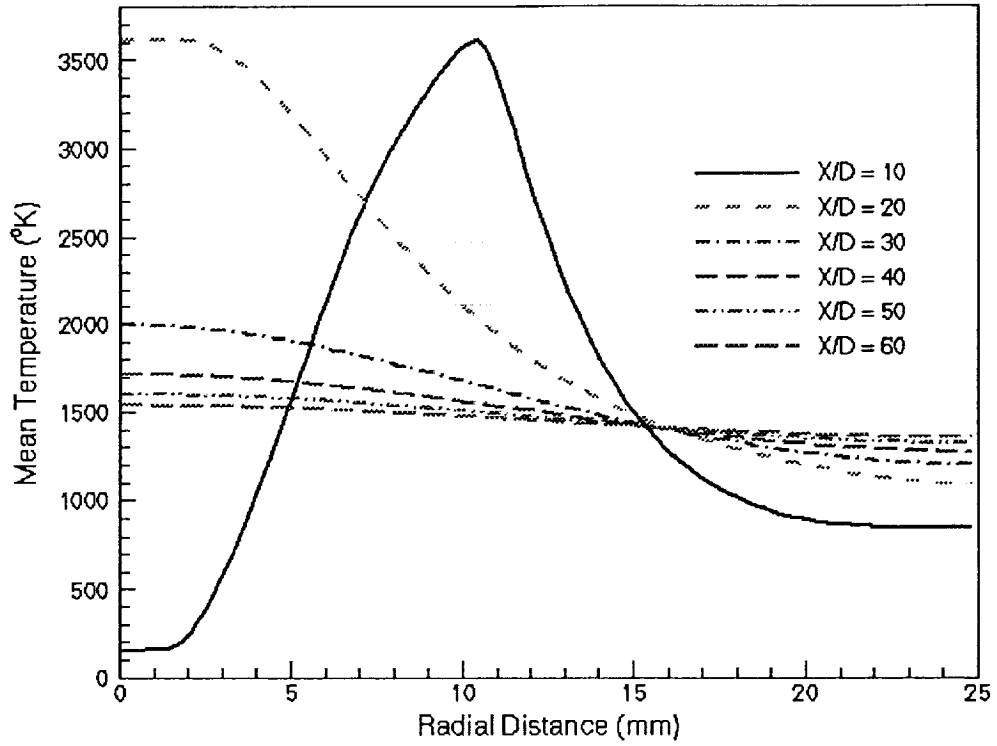


Figure 39 Radial Profiles of Mean Temperature at Various Axial Locations of RCM-3

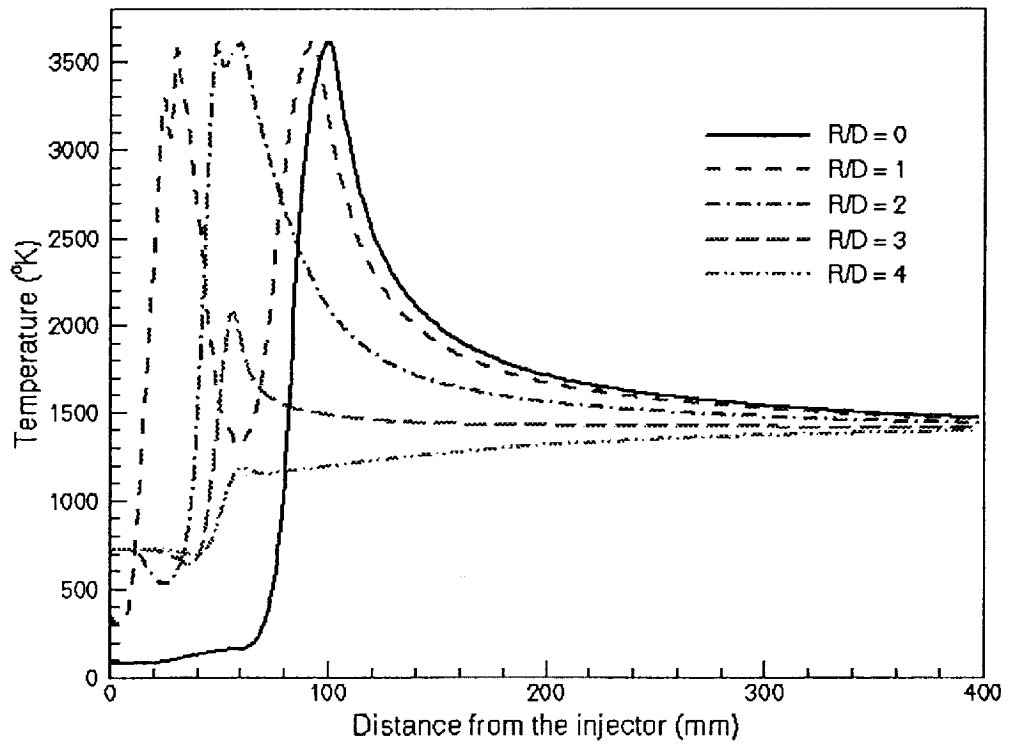


Figure 40 Axial Profiles of Mean Temperature at Various Radial Locations of RCM-3

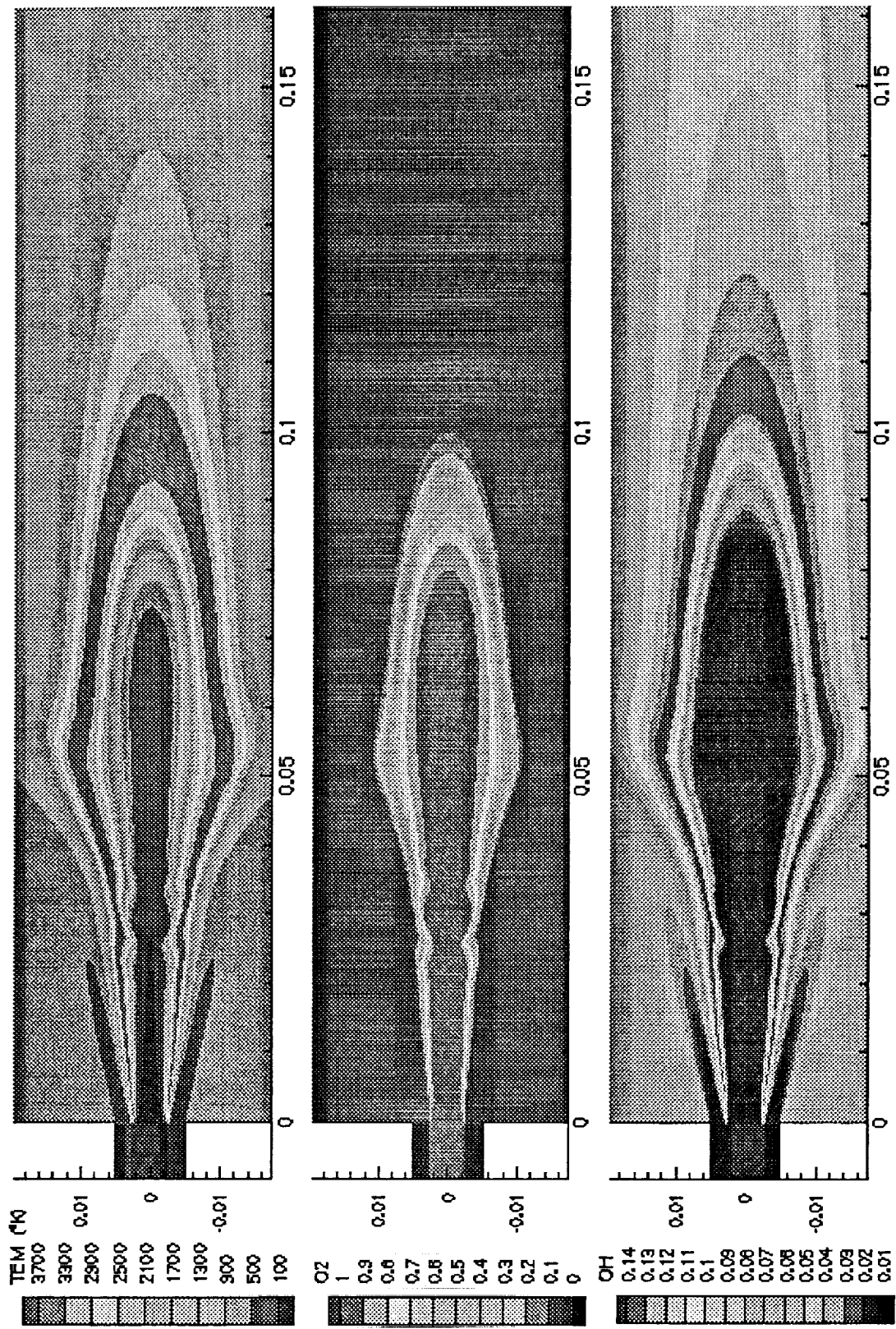


Figure 41 Temperature and Species Concentrations Near the Injector of RCM-3

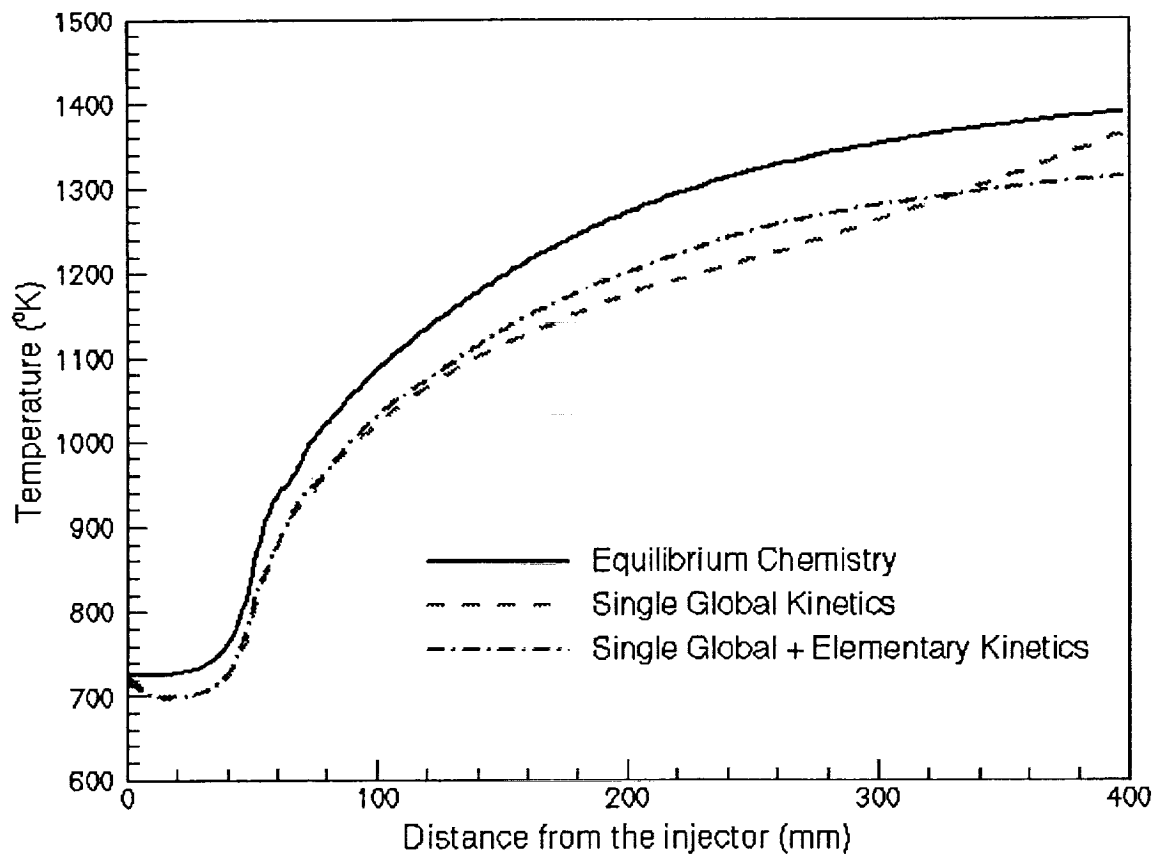


Figure 42 Near Wall Temperature Distributions for Various Chemistry Model of RCM-3

CONCLUSIONS

The following conclusions were drawn from performing CFD simulations of the three RCM test cases for the 2nd IWRCM.

1. A homogeneous and a heterogeneous spray combustion CFD model have been developed to simulate combustion in rocket engines. Since neither of these models is expected to be accurate until critical parameters are evaluated from test data, simulation comparisons to the MASCOTTE type experiments are needed.
2. The utility of either CFD model cannot be determined until values of critical parameters are determined and efforts to optimize the computational efficiency of the models are performed.
3. Although the CFD rocket engine models provide much more detailed information concerning the vaporization, mixing, and combustion process, their place in the design process is yet to be identified. Older more approximate rocket "performance" models are difficult to displace. Furthermore, every physical process thought to be present in the engine does not have to be modeled to create a useful design code. There are more knobs to adjust in the code than there are experimental data to justify their turning.
4. The experiments conducted in preparation for the 2nd IWRCM appear to be a significant first step in providing test data valuable to CFD modelers. However, blind comparisons of CFD model predictions to such data are premature. The CFD modelers have not previously had sufficient test data properly specify the many assumptions which are necessary to simulate such complex flows.
5. Better communication between analysts and experimenters needs to be accomplished. Can the modeler simulate the experiments which are being performed? Can the data obtained from the experiment critically test the model?

ACKNOWLEDGEMENTS

The authors wish to express their appreciation to Mr. Robert Garcia and Dr. Bill Anderson for their encouragement and support. This work was performed under NAS8-00162 for the Marshall Space Flight Center of the National Aeronautics and Space Administration.

REFERENCES

1. Chen, Y.S., "Compressible and Incompressible Flow Computations with a Pressure Based Method," AIAA Paper 89-0286, 1989.
2. Nickerson, G.R., et al, "Two-Dimensional Kinetics (TDK) Nozzle Performance Computer Program," Vols. I-III, Rpt. No. SN91, Software and Engineering Associates, Inc., mar. 1989.
3. Hirschfelder, J.O., et al, "Generalized Equations of State for Gases and Liquids," IEC, 50, pp.375-385, 1958.
4. Hirschfelder, J.O., et al, "Generalized Excess Functions for Gases and Liquids," IEC, 50, pp.386-390, 1958.
5. Reid, R.C., et al, The Properties of Gases & Liquids, 4th ed, McGraw-Hill, 1987.
6. Gordon, S., and B.J. McBride, "Computer Program for Calculation of Complex Chemical Equilibrium Compositions, Rocket Performance, Incident and Reflected Shocks, and Chapman-Jouget Detonations," NASA-SP-273, 1971.
7. Gardiner, W.C., Jr., Combustion Chemistry, Springer-Verlag, 1984.
8. Gardiner, W.C., Jr., Ed., Gas-Phase Combustion Chemistry, Springer, 1999.
9. Farmer, R.C, G. Cheng, H. Trinh, and K. Tucker, "A Design Tool for Liquid Rocket Engine Injectors," AIAA 2000-3499, 2000.
10. Reitz, R. D., and Diwakar, R., "Structure of High-Pressure Fuel Sprays," SAE Paper 860469, 1986.
11. Chen, Y. S., Shang, H. M., and Liaw, P., "A Fast Algorithm for Transient All-Speed Flows and Finite-Rate Chemistry," AIAA Paper 96-4445, 1996 AIAA Space Programs and Technologies Conference, September 24-26, 1996, Huntsville, AL.
12. O'Rourke, P. J., and Amsden, A. A., "The TAB Method for Numerical Calculation of Spray Droplet Breakup," SAE Paper 872089, 1987.
13. Shang, H. M., "Numerical Studies of Spray Combustion in Liquid-Fueled Engines," Ph.D. Thesis, University of Alabama in Huntsville, 1992.
14. Schuman, M. D., "General Evaporation Model," CDR-88-054, Rockwell International Corp., Feb. 1988.
15. Abramzon, B., and Sirignano, W. A., "Droplet Vaporization Model for Spray Combustion Calculations," AIAA Paper 88-0636, 1988.
16. Anon, "Spray Combustion of Synthetic Fuels, Phase II - Spray Combustion Phenomena," DOE/PC40276-5, SAI, Inc., Chatsworth, CA, May 1983.
17. Chehroudi, B., et al, "Initial Growth Rate and Visual Characteristics of a Round Jet into a Sub-to Supercritical Environment of Relevance to Rocket, Gas Turbine, and Diesel Engines," AIAA 99-0206, 1999.
18. Pope, S.B., Turbulent Flows, Cambridge, 2000.